Theoretical investigation of the autoionization process in molecular collision complexes: Computational methods and applications to $He^*(2^3S) + H(1^2S)$

M. Movre[a] and W. Meyer
Fachbereich Chemie, Universität Kaiserslautern, D-67663 Kaiserslautern, Federal Republic of Germany

(Received 29 October 1996; accepted 22 January 1997)

The first complete *ab initio* treatment is applied to the autoionization process in the $He^*(2s^3S) + H(1s)$ collisional complex. The autoionizing resonance state is defined through Feshbach projection based on orbital occupancy, and the corresponding potential is determined from multireference–configuration interaction (MR-CI) calculations with an accuracy of about 10 meV. The energy-dependent coupling with the continuum is derived from a compact (L^2) molecular orbital (MO) without any phase information being lost. This ''Penning MO'' is projected onto the states of the continuum electron for energies that comply with the resonance condition thus providing the l-dependent coupling elements in local approximation. The continuum electron functions are calculated within the static-exchange approximation for up to 25 coupled angular momentum channels. The nuclear dynamics calculation is based on a complex Numerov algorithm and uses a converged set of seven complex coupling matrix elements. Weighting with experimental collision energy distributions finally gives the angle-dependent, as well as the angle-integrated, electron spectra for Penning and associative ionization processes. The results are discussed with respect to previous, either partial or model studies, and are compared with the recent most detailed experimental study of the angular-dependent Penning ionization electron spectra. The close agreement of theory and experiment demonstrates the adequacy of the local complex potential approach, as well as the importance of electron angular momentum transfer so far neglected in theoretical treatments. © *1997 American Institute of Physics.* [S0021-9606(97)00417-0]

I. INTRODUCTION

The broad variety of processes that may occur in atomic collisions includes the ejection of free electrons. Such collisional autoionization processes are of particular complexity and have been studied extensively ever since they were first observed by Penning.[1] For a comprehensive review of recent research in this active field, we may refer to the excellent article by Siska.[2] Most of the autoionizing atomic (and molecular) collisions involve an excited atom. In this case, the Penning ionization (PI) process

$$A^* + B \rightarrow A + B^+ + e^- \tag{1}$$

is possible even in the limit of zero kinetic collision energy, provided only that the excitation energy of A is larger than the ionization potential of B. If the positive ion AB^+ has bound rovibrational states, the accompanying process of associative ionization (AI)

$$A^* + B \rightarrow AB^+ + e^- \tag{2}$$

is usually also observed. In cases of low excitation energies, it may even be the only energetically allowed ionization process.

Autoionization processes are of practical relevance as efficient energy redistribution mechanisms in discharges, laser plasmas,[3] as well as planetary atmospheres and interstellar clouds.[4] They also play a significant role as loss processes in laser cooling and atom trapping experiments.[5] Moreover, they are of genuine theoretical interest as they involve coupling mechanisms between electron and nuclear motion under the special circumstances of two coupled continua, that of the escaping electron and that of the colliding heavy particles. The proper treatment of the dynamics is still far from routine in such cases, and recent high-resolution electron spectra pose a new challenge to theoretical analysis and the development of adequate computational procedures.

For autoionization to occur with appreciable probability, the lifetime with respect to decay by electron emission should be less than or comparable to the collision time. Some of the most prominent collision systems in this field of research involve metastable states of rare-gas atoms for which autoionization is generally the dominant decay channel.[2] They offer several convenient properties, most notably of course their large excitation energies, which exceed the ionization potentials of most atoms and molecules. Upon approaching the collision partner, the metastable states evolve gradually into rather clean core-excited (Feshbach) resonance states, the widths of which grow more or less proportional to interatomic exchange, i.e., basically exponentially with decreasing distance. Therefore, collisions that surmount the centrifugal barrier decay by ionization with high probability and emit electrons of relatively large energies so that electron threshold effects are usually absent. From the theoretical point of view, this means that for thermal collision energies the ionization process can be treated safely within the Born–Oppenheimer approximation. Moreover, the elec-

[a]Permanent address: Institute of Physics of the University, HR-10000 Zagreb, Croatia.

tronic continuum is sufficiently complete and unstructured that the ionization can be viewed as a (vertical) Frank–Condon transition between a resonance state, conveniently defined by Feshbach projection,[6] and the continuum states. This relates the electron energy closely to the difference of the potentials at the internuclear separation where the ionization takes place. The entrance channel nuclear motion is then governed by a local complex potential. Its imaginary part is related to the local autoionization width and accounts for the loss of entrance channel population by ionization.

The theory of both, Penning and associative ionization, was fully developed in the seventies. Following the Feshbach projection operator approach as devised earlier by O'Malley[7] for the treatment of dissociative attachment, Nakamura,[8] Miller,[9] and Bieniek[10] presented detailed semiclassical, as well as fully quantum mechanical treatments, including the local approximation to the theory. Applications of the full nonlocal theory appear to have been restricted to a few bound molecules with electronic shape resonances where collisions with slow electrons invalidate the local approximation.[11] But even in the local approximation, for which the validity range has recently been discussed by Morgner,[12] only few quantitative applications have so far appeared in the literature. All of them are restricted to some of the aspects of the complete theory, either just considering the motion in the entrance channel or calculating differential cross sections by using model potentials and width functions in conjunction with approximate scattering treatments. (For more details, we refer again to the review by Siska,[2] and references therein.) To some extent, modeling the resonance-to-continuum coupling was enforced by the nearly complete lack of information on the individual coupling matrix elements between the resonance state and the specific final states corresponding to outgoing electrons with angular momentum quantum numbers l and m. To our knowledge, the calculation of such individual coupling elements has been attempted only for the Penning systems He*+H, H_2 by Miller and co-workers,[13,14] but this work involved severe approximations in the representation of the continuum electron and did not result in a simple picture for phase relations among the coupling elements and their dependence on internuclear separation. More reliable data were available for the total autoionization width, generally showing a rather smooth and nearly exponential dependence on R. In addition, the restriction to approximate scattering treatments based only on total width functions seemed justified, as all prominent features of the Penning electron spectra could be understood or even reasonably well reproduced by semiempirical models of the width function, even though these shortcuts effectively removed any angular momentum transfer to the electron from the theory.

The recent high-resolution electron spectra for Penning systems with attractive interaction potentials such as He*+H, Li, Na, Rb, and Cs,[15,16] etc., made it, however, apparent that their rich interference structure cannot be accounted for adequately without highly accurate resonance potentials, as well as detailed data for l-dependent coupling elements, including their phases.

Our own efforts for a theoretical analysis and a reliable calculation of autoionization electron spectra were first directed towards the adiabatic potentials of the resonance states. It could be demonstrated for the systems mentioned above,[15,16] as well as He*+He*,[17] that these resonance potentials can be obtained with an accuracy of about 10 meV for the depth of the well by implementing Feshbach projection in *ab initio* multireference configuration interaction (MR-CI) methods.[18] From this type of calculation, we have then obtained width functions with an estimated accuracy of 10% by familiar Stieltjes imaging procedures.[19,20] Using these potentials and widths in the approximate scattering treatment usually adopted so far yielded excellent agreement with experiment for properties such as the position of the main Airy peak (which reflects the depth of the well) and total ionization cross sections (which sensitively probe the long-range tail of the potential).[21] However, we did not obtain satisfying agreement with experiment for the shape of the main peak, the detailed interference pattern and the overall resolution of the spectra. This could be significantly improved only when employing the full local scattering theory with certain model assumptions for the l-dependent coupling elements, and a significant angular dependence of the electron spectra was predicted even for systems that have a relatively strong attractive resonance potential.[21] The spectra of such systems have usually been assumed to be essentially isotropic, and spectra taken under 90° perpendicular to the atomic beams were normally compared with spectra calculated from angle-integrated formulas.[2] The angular dependence of such electron spectra has recently been verified by the high-resolution electron spectrometry measurements due to Hotop and co-workers.[21–23]

Our attempts to obtain reliable l-dependent coupling elements from the convenient Stieltjes procedure were not successful, however, mainly because they depend sensitively on the long-range electronic potential in the ionic exit channel. Therefore, one cannot trust an expansion of the continuum electron wave function in terms of the L^2 Gaussian-type orbitals (GTOs) to which quantum chemical programs are usually restricted. It may be pointed out here that for a system such as He*+Li, electrons of energies around 13 eV (that is, with de Broglie wavelengths of about 6 bohr) are ejected mainly from a region close to the He 1s core and then move in a Coulomb field that is centered 4–10 bohr away. Their wave function involves partial waves up to $l \leqslant 8$ for an asymptotic expansion with respect to the center of mass. Therefore, it appears unavoidable to resort to a numerical description of the continuum electron as common in electron scattering codes. For the systems under consideration here, it is certainly adequate to apply the static-exchange approximation.[24] In this paper, we give a detailed description of a two-step procedure by which all pertinent information on the resonance–continuum coupling is first compressed into a bound one-electron function, which we may call the Penning molecular orbital (MO). This MO is obtained by making full use of modern direct CI techniques for electron structure calculations with extensive GTO basis sets, and it does not, at one point or other, require full diagonalization in some

large configuration space. It is a bound MO by nature and not by basis set restrictions and, therefore, it is subject only to the usual errors of a finite CI expansion. This MO is expressed in the form of a numerical partial wave expansion and then projected onto the solutions of proper energy from static exchange electron scattering calculations in a configuration space that is orthogonal to that used in the calculation of the resonance state. This provides the complex coupling elements that complete the electronic structure input to the equations for nuclear motion and electron distribution. We are, thus, in a position to carry out a purely *ab initio* treatment of the autoionization process with only the local complex potential approximation.

We exemplify all the computational procedures involved by calculations for the collision system $He^*(2s^3S)+H(1s)$, which is the simplest and most fundamental among the numerous autoionizing collision complexes. In the last two decades the system He^*+H has been intensively studied in the thermal energy range both theoretically and experimentally, and it has indeed become a benchmark system. The most detailed information is provided by electron spectrometry, which has culminated in the very recent studies of the angular dependence of the spectra, performed with high energy resolution ($\sim$ 30 meV) and improved signal-to-noise ratio by Merz and co-workers.[21–23] This has been extended to collisions involving D, as well as $He^*(2s^1S)$.[25,26] Pioneering theoretical work on this system includes the calculation of the resonance state potential by the stabilization method,[27] the Feshbach projection operator method,[14] and the Siegert complex eigenvalue method.[28] The former two methods have also been applied in an attempt to derive individual coupling matrix elements.[13,14] They have subsequently been used (and criticized) in a coarse simulation of electron spectra.[10] In more recent numerical simulations of observed spectra, our *ab initio* resonance potential[15,21] has already been applied and has been found to be superior to all previously reported potentials. However, clear discrepancies between the shapes of our width functions from Stieltjes imaging and the best-fit empirical width functions remained unresolved. Our first results for complex l-dependent coupling elements have been published in the context of brief comparisons between measured and calculated spectra.[29,25] Resonance potential, width function, and internal angular distributions (for three selected internuclear distances) have also been derived from R-matrix electron scattering calculations.[30]

This paper is organized in the following way: In Sec. II we briefly review the formal theory of the autoionization processes. In Sec. III we discuss our computational procedures for the five steps involved in the calculation of the electron spectra, i.e., (i) the definition of the resonance state by Feshbach projection, (ii) the *ab initio* calculation of the potential curves and the ''Penning MO,'' (iii) the calculation of continuum states in static exchange approximation and the derivation of the complex coupling coefficients, (iv) the heavy particle dynamics in the complex potential, and (v) the calculation of electron intensities. The performance of the Feshbach projection approach for resonance energies, as well as coupling elements, is also exemplified for two related atomic resonances. Section IV presents computational details and results for $He^*(2^3S)+H$, and in Sec. V we discuss our angle-dependent spectra in comparison with previous work and experiment.

II. CONCEPT OF THE FORMAL THEORY

A. Feshbach projection operator method

Neither the state A^*+B nor the states $A+B^++e^-$ are eigenstates of the total electronic Hamiltonian $H_{\rm el}$. It is through interaction by $H_{\rm el}$ with the continuum of states $A+B^++e^-$ that the state A^*+B autoionizes,[9,10] that is, the state A^*+B is a ''resonance state.'' In many cases, this interaction is rather weak and the resonance structure is relatively long living. It is then desirable to solve the problem in two steps.

According to the original Feshbach treatment,[6] one defines two complementary projection operators P and $Q=1-P$, which partition the electronic Hilbert space into two subspaces, one containing the relevant ''background continuum'' states and the other containing the ''bound,'' resonance or autoionizing state(s). The continuum states describe asymptotically the ground or low-lying excited eigenstates of the ionized molecular complex and a free electron ejected with energy ϵ in the direction $\hat{\omega}$. Considering only a single electronic exit channel for simplicity, the projection P may be written as

$$P=\int d\boldsymbol{\epsilon}|\phi_{\boldsymbol{\epsilon}}\rangle\langle\phi_{\boldsymbol{\epsilon}}|, \tag{3}$$

where $\boldsymbol{\epsilon}=\epsilon\hat{\omega}$. The total (electronic and nuclear) wave function $\psi_E=P\psi_E+Q\psi_E$ is the solution of the coupled equations

$$P(\hat{H}-E)P\psi_E=-P\hat{H}Q\psi_E, \tag{4}$$

$$Q(\hat{H}-E)Q\psi_E=-Q\hat{H}P\psi_E. \tag{5}$$

The Q-space part of a scattering solution with proper outgoing boundary conditions is given by

$$Q(\hat{H}-E)Q|\psi_E^{\rm out}\rangle=-Q\hat{H}P(E-\hat{H}+i\delta)^{-1}P\hat{H}Q|\psi_E^{\rm out}\rangle. \tag{6}$$

For an adequate choice of projection operators, it is assumed that the subspaces vary slowly with internuclear separation and then nonadiabatic coupling between them is negligible. In the case of an isolated resonance state, we may assume a single (Born–Oppenheimer) product of an electronic wave function $|\phi_*\rangle$ and a nuclear wave function $|\chi_*^{\rm out}\rangle$

$$Q|\psi_E^{\rm out}\rangle=|\phi_*\rangle|\chi_*^{\rm out}\rangle. \tag{7}$$

For the solution of the homogeneous equation in the exit channel, we assume similarly

$$P|\psi_E^o\rangle=|\phi_{\boldsymbol{\epsilon}}\rangle|\chi_{\mathbf{E}_+}\rangle, \tag{8}$$

where $E_++\epsilon=E$, and $\mathbf{E}_+=E_+\hat{\Omega}_+$ denotes the energy and asymptotic direction of the motion of the ionized complex. The electronic wave function behaves asymptotically as the

product of the ground-state wave function of the ionized complex and a free electron function, $\phi_{\boldsymbol{\epsilon}} \rightarrow \Phi_+ \varphi_{\boldsymbol{\epsilon}}$.

With the exit channel potential defined as $V_+ = \langle \Phi_+ | H_{\rm el} | \Phi_+ \rangle$, the exit channel nuclear wave function is the solution of

$$|\hat{T}_N + V_+ - E_+ | \chi_{\mathbf{E}_+} \rangle = 0. \tag{9}$$

Multiplying Eq. (6) by $\langle \phi_* |$, one obtains for the entrance channel nuclear wave function

$$\begin{aligned} &|\hat{T}_N + V_* - E | \chi_*^{\rm out} \rangle \\ &\quad = -\langle \phi_* | \hat{H} P (E - \hat{H} + i\delta)^{-1} P \hat{H} | \phi_* \rangle | \chi_*^{\rm out} \rangle \\ &\quad = -|\hat{\Delta} - \frac{1}{2}\hat{\Gamma} | \chi_*^{\rm out} \rangle, \end{aligned} \tag{10}$$

where $\hat{\Delta}$ and $\hat{\Gamma}$ are the energy-dependent shift and width operators and $V_* = \langle \phi_* | H_{\rm el} | \phi_* \rangle$ is the entrance channel (resonance) potential. Introducing a complete set of energy-normalized nuclear wave functions

$$\int d\mathbf{E}_+ | \chi_{\mathbf{E}_+} \rangle \langle \chi_{\mathbf{E}_+} | = 1, \tag{11}$$

and using P as defined in Eq. (3), $\hat{\Delta}$ and $\hat{\Gamma}$ can be expressed as

$$\hat{\Gamma}(E) = 2\pi \int d\boldsymbol{\epsilon} \int d\hat{\Omega}_+ V_{\boldsymbol{\epsilon}}^* | \chi_{\mathbf{E}_+} \rangle \langle \chi_{\mathbf{E}_+} | V_{\boldsymbol{\epsilon}}, \tag{12}$$

$$\hat{\Delta}(E) = \frac{1}{2\pi} \mathscr{P} \int dE' \, \frac{\hat{\Gamma}(E')}{E - E'}, \tag{13}$$

where the coupling matrix elements are defined as

$$V_{\boldsymbol{\epsilon}}(\mathbf{R}) = \langle \phi_{\boldsymbol{\epsilon}} | \hat{H} | \phi_* \rangle. \tag{14}$$

$\hat{\Delta}$ and $\hat{\Gamma}$ can be converted into a local potential if some reasonable approximations are justified. Noting that the use of Eq. (12) in Eq. (10) results in an integral over a product of two fast-oscillating nuclear wave functions, the usual stationary-phase condition leads to the conservation of nuclear kinetic energy and the Franck–Condon resonance condition for a vertical transition at R_v,

$$\boldsymbol{\epsilon}_v = \boldsymbol{\epsilon}(R_v) = V_*(R_v) - V_+(R_v). \tag{15}$$

If threshold electrons can be excluded (i.e., V_* and V_+ do not come close), it may also be assumed that $V_{\boldsymbol{\epsilon}}(\mathbf{R})$ is only weakly dependent on the electron energy $\boldsymbol{\epsilon}$ around the vertical energy $\boldsymbol{\epsilon}_v$ and that it may be substituted by a constant $V_{\boldsymbol{\epsilon}_v}(\mathbf{R}_v)$ in Eq. (12). The integral then turns into a projector to the energetically allowed exit channel vibrational functions, which acts as unity on $|\chi_*^{\rm out}\rangle$ since the allowed kinetic energies in the exit channel are larger than the maximum kinetic energy in the entrance channel. Under these conditions, the effective potential in Eq. (10) turns out to be local,

$$V_{\rm opt}(R) = V_*(R) + \Delta(R) - \frac{i}{2}\Gamma(R), \tag{16}$$

where the width $\Gamma(R)$ and the shift $\Delta(R)$ are given as

$$\Gamma(R) = 2\pi \int d\hat{\omega} |V_{\boldsymbol{\epsilon}}(\mathbf{R})|^2 |_{\boldsymbol{\epsilon} = \boldsymbol{\epsilon}_v(R)}, \tag{17}$$

$$\Delta(R) = \mathscr{P} \int d\boldsymbol{\epsilon}' \, \frac{|V_{\boldsymbol{\epsilon}'}(\mathbf{R})|^2}{\boldsymbol{\epsilon}_v(R) - \boldsymbol{\epsilon}'}. \tag{18}$$

B. Differential cross sections

The most detailed cross section for the process under consideration is triple differential: in the asymptotic direction $\hat{\omega}$ of the ejected electron, in the asymptotic direction $\hat{\Omega}_+$ of the outgoing heavy particle system $A + B^+$, and, due to energy conservation, in one of the asymptotic energies, either that of the electron or that of the molecular ion.

In terms of the T-matrix elements for the transition from an initial state i (entrance channel) to a final state f (exit channel), the differential cross section is given by[10]

$$\frac{d^3\sigma}{d\epsilon d\hat{\omega} d\hat{\Omega}_+} = g_* \, \frac{(2\pi)^4}{k_i^2} \, |T_{fi}|^2 \delta(E_i - E_f). \tag{19}$$

Here, g_* is the statistical weight of the entrance channel, k_i is the asymptotic wave vector of the entrance channel motion, and the T-matrix element is defined as

$$T_{fi} = \langle \chi_{\mathbf{E}_+}^{\rm in} | V_{\boldsymbol{\epsilon}'} | \chi_*^{\rm out} \rangle. \tag{20}$$

The standard procedure to evaluate T-matrix elements is to expand the scattering wave functions into partial waves composed of the product of angular and radial functions. For the entrance channel nuclear wave function, one writes

$$\chi_*^{\rm out}(\mathbf{R}) = \sum_{JM} Y_{JM}^*(\hat{\Omega}) Y_{JM}(\hat{R}) i^J F_J(R) R^{-1}. \tag{21}$$

Here, $\hat{\Omega}$ is the incident beam direction with respect to an arbitrarily oriented space-fixed coordinate system. The radial wave function F_J for the entrance channel nuclear motion is the solution of the radial wave equation with a complex potential

$$\begin{aligned} &\left(-\frac{\hbar^2}{2\mu} \frac{d^2}{dR^2} + V_*(R) + \Delta(R) - \frac{i}{2}\Gamma(R) \right. \\ &\quad \left. + \frac{\hbar^2}{2\mu} \frac{J(J+1)}{R^2} - E \right) F_J(R) = 0, \end{aligned} \tag{22}$$

where μ is the reduced mass. An expression analogous to Eq. (21) holds for the nuclear wave function of the exit channel cation. The corresponding radial wave function $F_{J'}^+$ obeys

$$\left(-\frac{\hbar^2}{2\mu} \frac{d^2}{dR^2} + V_+(R) + \frac{\hbar^2}{2\mu} \frac{J'(J'+1)}{R^2} - E_+ \right) F_{J'}^+(R) = 0. \tag{23}$$

Both radial wave functions are taken to be energy normalized and behave asymptotically as

$$F_J(R) \sim \left(\frac{2\mu}{\pi\hbar^2 k} \right)^{1/2} e^{i\eta_J} \sin\left(kR - J\frac{\pi}{2} + \eta_J \right). \tag{24}$$

The phase shifts η_J pertinent to the entrance channel with complex potential are necessarily also complex. Note that the factor $e^{i\eta_J}$ is here taken as part of $F_J(R)$.

As the continuum electronic wave function is assumed to involve only one channel connected with the electronic ground state of the cation, Φ_+, for linear collision complexes it may be expanded as

$$\phi_{\boldsymbol{\epsilon}}=\hat{A}\Phi_+\varphi_{\boldsymbol{\epsilon}}=\hat{A}\Phi_+\sum_{lm} i^l Y^*_{lm}(\hat{\omega}_{\hat{R}})\varphi_{\epsilon lm}(\mathbf{r}_{\hat{R}}), \tag{25}$$

where $\hat{A}$ antisymmetrizes the product of Φ_+ with the continuum electron function. As indicated by the subscript $\hat{R}$, the partial waves refer to the molecule fixed coordinate system. Since the continuum electron moves in an anisotropic potential, its wave function should further be expanded as

$$\varphi_{\epsilon lm}(\mathbf{r}_{\hat{R}})=\sum_{l'} Y_{l'_m}(\hat{r}_{\hat{R}})f_{\epsilon ll'}(r)r^{-1}. \tag{26}$$

With $k_e=\sqrt{2m_e\epsilon/\hbar}$, the asymptotic boundary condition for $f_{\epsilon ll'}(r)$ is

$$f_{\epsilon ll'}(r)\sim\delta_{ll'}\left(\frac{2m_e}{\pi\hbar^2 k_e}\right)^{1/2} e^{i\eta_l}\sin\left(k_e r+k_e^{-1}\ln(2k_e r)-l\frac{\pi}{2}+\eta_l\right). \tag{27}$$

The complex phase factor in the radial function $f_{\epsilon ll'}(r)$ is partly due to the Coulomb phase shift in a field of unit positive charge at B^+ and partly due to the atomic potential(s) of A and B^+. [We point out in passing that in Bieniek's[10] and other previous treatments the right-hand side (rhs) of Eq. (26) was reduced to a single term $l'=l$, supposing a pure Coulomb wave.]

Substituting Eq. (26) in Eq. (25) results in

$$V_{\boldsymbol{\epsilon}}(\mathbf{R})=\sum_l i^{-l}Y_{lm}(\hat{\omega}_{\hat{R}})V_{\epsilon l}(R), \tag{28}$$

where $V_{\epsilon l}(R)$ are complex partial wave components of the coupling matrix element $V_{\boldsymbol{\epsilon}}(\mathbf{R})$ given by

$$V_{\epsilon l}=\langle\hat{A}\phi_+\varphi_{\epsilon lm}(\mathbf{r}_{\hat{R}})|\hat{H}_{el}|\phi_*\rangle. \tag{29}$$

They build up the total width function $\Gamma(R)$ as given by Eqs. (17) and (27), that is, $\Gamma_{\boldsymbol{\epsilon}}(R)=2\pi\Sigma_l|V_{\epsilon l}(R)|^2$. The $V_{\epsilon l}$ are directly related to the so-called internal angular distribution of the emitted electron. For a specific internuclear separation R, it is given by

$$P_{\rm int}(\theta,R)=|V_{\boldsymbol{\epsilon}_v}(\mathbf{R})|^2=\left|\sum_l i^{-l}V_l(R)Y_{lm}(\theta,0)\right|^2, \tag{30}$$

where θ represents the body-fixed electron scattering angle. We point out that the index $\boldsymbol{\epsilon}$ is dropped from $V_{\epsilon l}(R)$ if $\boldsymbol{\epsilon}$ is determined by the resonance condition (15).

For angular integrations in the T matrix, all angles should refer to the center-of-mass (c.m.) coordinate system. Transformation of Eq. (28) to the c.m. system introduces a Wigner rotation matrix (of argument $\hat{R}$), which reduces to a spherical harmonic if the emitted electron is a σ electron ($m=0$), which we may assume for the following. The T-matrix element (20) is then given by[10]

$$T_{fi}=\frac{1}{\sqrt{4\pi}}\sum_{J'M}\sum_{lm}\sum_J Y_{J'M}(\hat{\Omega}_+)Y_{lm}(\hat{\omega})\times\begin{pmatrix}J' & l & J\\ M & m & 0\end{pmatrix}C_{J'lJ}\langle F^+_{J'}|V_l|F_J\rangle, \tag{31}$$

where

$$C_{J'lJ}=i^{J-J'-l}(2J'+1)^{1/2}(2J+1)\begin{pmatrix}J' & l & J\\ 0 & 0 & 0\end{pmatrix}. \tag{32}$$

Integrating Eq. (19) over the angles of the ejected electron, one obtains the double differential cross section describing the energy and angle distribution of the heavy particles ($A+B^+$) in the exit channel,

$$\frac{d^2\sigma}{dE_+ d\hat{\Omega}_+}=g_*\frac{4\pi^3}{k_i^2}\sum_{lm}\left|\sum_{J'J}\begin{pmatrix}J' & l & J\\ -m & m & 0\end{pmatrix}\times Y_{J'm}(\hat{\Omega}_+)C_{J'lJ}\langle F_{J'}|V_l|F_J\rangle\right|^2. \tag{33}$$

Integrating Eq. (19) over the angles of the product nuclei, one obtains the double differential cross section describing the energy and angle distribution of the ejected electron,

$$\frac{d^2\sigma}{d\epsilon d\hat{\omega}}=g_*\frac{4\pi^3}{k_i^2}\sum_{J'M}\left|\sum_{Jl}\begin{pmatrix}J' & l & J\\ -M & M & 0\end{pmatrix}\times Y_{lM}(\hat{\omega})C_{J'lJ}\langle F^+_{J'}|V_l|F_J\rangle\right|^2. \tag{34}$$

By expanding the absolute square[31,32] one can transform this equation into a form that is somewhat more convenient for analysis of angular dependence:

$$\frac{d^2\sigma}{d\epsilon d\hat{\omega}}=g_*\frac{\pi^2}{k_i^2}\sum_L(2L+1)A_L(\epsilon)P_L(\cos\theta), \tag{35}$$

where

$$A_L(\epsilon)=\sum_{J'}\sum_{J_1J_2}\sum_{l_1l_2}(-1)^{J'+l_1-l_2}\begin{pmatrix}J_1 & J_2 & L\\ 0 & 0 & 0\end{pmatrix}\times\begin{pmatrix}l_1 & l_2 & L\\ 0 & 0 & 0\end{pmatrix}[(2l_1+1)(2l_2+1)]^{1/2}\times\begin{Bmatrix}J_1 & J' & l_1\\ l_2 & L & J_2\end{Bmatrix}C^*_{J'l_2J_2}C_{J'l_1J_1}\times\langle F_{J_2}|V^*_{l_2}|F^+_{J'}\rangle\langle F^+_{J'}|V_{l_1}|F_{J_1}\rangle. \tag{36}$$

The angular dependence of the integrated electron intensity is then obtained as

$$\frac{d\sigma}{d\hat{\omega}}=g_*\frac{\pi^2}{k_i^2}\sum_L(2L+1)\overline{A_L}P_L(\cos\theta), \tag{37}$$

where

$$\overline{A_L}=\sum_{J_1J_2}\sum_{l_1l_2} i^{J_1-J_2+l_2-l_1}(2J_1+1)(2J_2+1)$$
$$\times[(2l_1+1)(2l_2+1)]^{1/2}\begin{pmatrix} J_1 & J_2 & L \\ 0 & 0 & 0\end{pmatrix}^2$$
$$\times\begin{pmatrix} l_1 & l_2 & L \\ 0 & 0 & 0\end{pmatrix}^2\langle F_{J_2}|V_{l_2}^{*}V_{l_1}|F_{J_1}\rangle. \quad (38)$$

The differential cross section describing the angle-integrated energy distribution of the ejected electron is given by

$$\frac{d\sigma}{d\epsilon}=g_*\frac{4\pi^3}{k_i^2}\sum_{J'lJ}(2J'+1)(2J+1)$$
$$\times\begin{pmatrix} J' & l & J \\ 0 & 0 & 0\end{pmatrix}^2|\langle F_{J'}^{+}|V_l|F_J\rangle|^2. \quad (39)$$

Finally, the integration of Eq. (39) over ϵ yields the total ionization cross section, that is,

$$\sigma(E)=g_*\frac{\pi}{k_i^2}\sum_J (2J+1)O_J(E). \quad (40)$$

The opacities $O_J(E)$, the ionization probability per collision with angular quantum number J, are defined as $O_J(E)=\{1-\exp[-4\ \mathrm{Im}(\eta_J(E))]\}$, with $\eta_J(E)$ being the complex phase shift in the entrance channel.

From the knowledge of the entrance channel phase shifts η_J, one may also derive the differential elastic cross section for the atoms A^* and B,

$$\frac{d\sigma}{d\theta}=\frac{g_*}{4k_i^2}\left|\sum_J (2J+1)(e^{2i\eta_J}-1)P_J(\cos\theta)\right|^2. \quad (41)$$

C. Approximations

In the previous sections, we have reviewed the basic concepts of the formal theory of PI/AI processes. Clearly, for the full treatment of an autoionizing collision including the electron distribution, the knowledge of the partial matrix elements $V_l(R)$ is required besides $V_+(R)$ and $V_*(R)$. But one needs only the total width function $\Gamma(R)$ (17) in case one is interested just in quantities strictly related to the entrance channel, such as total ionization cross sections (40) or total and angle-dependent elastic scattering cross sections (41).

Lacking sufficient information on the individual coupling elements $V_l(R)$, the following approximations suggested by Hickman and Morgner[33] have commonly been used in the analysis of experimental electron spectra: The $V_l(R)$ are assumed to factorize into the supposedly known function $\Gamma(R)^{1/2}$ and functions $\alpha_l(R)$, which are assumed to vary slowly as compared to the radial wave functions. They then suppose that the integral is mainly due to contributions from a single point of stationary phase, as is the case for repulsive potentials, and approximate $\alpha_l(R)$ by its value at this point. For the angular dependence of energy-integrated electron intensities, this gives a product of two sums from which α parameters have been determined empirically for some repulsive collision systems,[32]

$$\overline{A_L}=\sum_{J_1J_2} i^{J_1-J_2}(2J_1+1)(2J_2+1)$$
$$\times\begin{pmatrix} J_1 & J_2 & L \\ 0 & 0 & 0\end{pmatrix}^2\left\langle F_{J_2}\left|\frac{\Gamma}{2\pi}\right|F_{J_1}\right\rangle\sum_{l_1l_2} i^{l_2-l_1}[(2l_1+1)$$
$$\times(2l_2+1)]^{1/2}\begin{pmatrix} l_1 & l_2 & L \\ 0 & 0 & 0\end{pmatrix}^2\alpha_{l_2}^{*}\alpha_{l_1}. \quad (42)$$

For simulations of electron energy distributions, the additional approximation $\langle F_{J'}^{+}|V_l|F_J\rangle\cong\langle F_J^{+}|V_l|F_J\rangle$, proposed previously by Bieniek[34] was adopted, which leads to

$$\frac{d\sigma}{d\epsilon}=g_*\frac{2\pi^2}{k_i^2}\sum_J (2J+1)|\langle F_J^{+}|\Gamma^{1/2}|F_J\rangle|^2. \quad (43)$$

It is important to note that this approximation effectively removes rotational transfer from the theory because $\Delta J=0$ is strictly compatible only with the assumption of an isotropic electron distribution, i.e., $l=0$ only. The widespread use of approximation (43) rests on two observations: First, this rather simple treatment does indeed reproduce the main structures of Penning electron spectra, provided that accurate potentials $V_*(R)$, $V_+(R)$ and a reasonable width $\Gamma(R)$ are used.[21] Second, $\Gamma(R)$ is normally a smooth monotonic function, an exponential in $(-R)$ leveling off at shorter R, which can be determined from quantum chemical calculations with relative ease, e.g., by Stieltjes imaging procedures, and which lends itself to semiempirical modeling. In particular, for repulsive systems (for which this approximation was first introduced) with electron spectra that show a dominant main Airy peak and little interference structure, the width function $\Gamma(R)$ provides sufficient flexibility to model the observed spectra with satisfactory success.[35] But semiempirical modeling via Eq. (43) has also been applied to attractive systems and their much more structured spectra, which are usually taken only at a 90° angle by sampling electrons in a direction perpendicular to the plane defined by two orthogonal atomic beams. As pointed out in Sec. II B, this was based on the widely accepted assumption that the laboratory frame electron angular distribution is basically isotropic for systems with an attractive entrance channel potential, where the rotation of the collision complex tends to smear out the direction of the internuclear axis.[15,16] However, even with an attractive potential, the autoionizing collision is, in fact, sufficiently direct for an inherently nonisotropic internal angular distribution of the ejected electron to be observable as an angular dependence of the laboratory-frame electron spectrum. Besides, rotational excitation or deexcitation during the autoionization process leads to shifts of the electron energies towards lower or higher values, respectively, since the points of the stationary phase are significantly different for the integrals involving different J' but the same J. The true angle-integrated distributions are, therefore, usually broader and less structured than the ones calculated by means of Eq. (43). This explains why better agreement is observed between

electron energy distributions calculated on the basis of Eq. (43) and spectra measured at $\theta=90°$ than with angle-integrated experimental spectra. Indeed, we found that for systems such as $He^*(2s^3S)+Li$ or Na, the $\Delta J=0$ approximation contained in Eq. (43) is best fulfilled for angles around 90°.[21,22] For $He^*(2s^3S)+H$, however, this kind of modeling was not very successful and the best-fit $\Gamma(R)$ exhibited a rather unlike shape.[15]

The approximation (43) was based on the assumption that there is only a single point of stationary phase. For an attractive potential V_*, as under consideration here, there are two stationary points, the interference of which is responsible for the typical Airy oscillations in the spectra. Still, some simple approximation for $V_l(R)$ may work fairly well if (i) the two points of stationary phase are very close so that the difference between the corresponding α_l can be neglected, or if (ii) they are very far from each other so that the phase relations interfere out, or if (iii) a steep exponential decrease of the V_l causes the inner point to dominate the integral. In previous work, we have explored simplifications for V_l in model studies incorporating rotational energy changes by adopting suitably chosen constants α_l for the V_l in Eq. (39) and fixing J by a prescribed $\Delta J=J'-J$.[21,22] Exploiting the interrelation of the electron detection angle with the preferred ΔJ values and the J range, which contributes dominantly to certain parts of the spectra as visible in classical trajectory calculations, some important aspects of the angular dependence of the electron spectra could be understood. Clearly, such a procedure is not really satisfying and mainly served to demonstrate the expected angular dependence of the spectra and to establish the need of individual coupling elements V_l. It should also be noted that the latter are indispensible to derive internal angular distributions of the ejected electrons, which are important for characterizing the ionization mechanism.

III. COMPUTATIONAL METHODS

The most rigorous procedure to derive V_* as well as $V_{\epsilon l}$ would certainly use phase-shift calculations by electron scattering techniques such as the R-matrix method. This is not a simple task for an ionizing collisional system with a very narrow resonance at rather high electron energies and with a Coulomb center that may be up to 10 bohr away from the region where the electron is ejected from, thus, requiring the coupling of many electron angular momenta. Considering that the highest priority should be given to accurate potentials $V_*(R)$ and that the electronic structure in the entrance channel is that of a (rather narrow) core-excited resonance, we decided to base our treatment on Feshbach projection and to proceed in several steps as outline in the introduction.

A. Definition of Feshbach projection schemes

As stressed by Feshbach,[6] the definition of the projection operators Q and P is by no means unique and provides a welcome flexibility for actual calculations. The necessary condition only requires that for the exact electronic wave function ψ_E

$$\lim_{r\to\infty} P\psi_E \to \psi_E , \tag{44}$$

where r denotes the radial coordinate of any of the electrons. This means that all asymptotically important information should be contained in the P-space part of the exact wave function, i.e., $P\psi_E$ asymptotically describes $AB^+ + e^-$. As a consequence, $\lim_{r\to\infty} Q\psi_E \to 0$, and any part of the Q space may be shifted to the P space, provided the requirement of negligible nonadiabatic coupling between the subspaces is obeyed. While the results of an exact treatment would not be affected by the particular choice of the projection, any approximation in the evaluation of the intermediate quantities such as ϕ_*, V_*, or $V_{\epsilon l}$ introduces some dependence on the projection scheme.

From the conceptual point of view, one would like to determine Q and P in a way so that ϕ_* represents a good approximation to the close-in part of the total wave function and the shift Δ becomes small. Then it may be justified to neglect the latter and to avoid evaluation of Eq. (18). To this end, one wants to keep Q as large as possible. Dealing with a finite one-electron basis set of L^2 functions, one may even define Q as projecting onto the entire $N-$electron configuration space that may be built from these functions. This is the spirit of the stabilization method as applied by Miller and Schaefer to He^*+H.[27] In this case, Q contains, in general, not only bound and genuine resonance states but also discretized continuum states where φ_ϵ takes the form of a wave packet describing a localized unbound electron. As long as the basis does not include diffuse functions, identification of resonances may simply be based on reference to the molecular dissociation limit.[27] Diffuse functions, however, are essential for an adequate description of the long-range part of the resonance potential that has a significant effect on the total cross section for low-energy PI processes. They lead to avoided crossings between resonance and quasicontinuum states. In standard applications of the stabilization method, an extended set of diffuse functions has been used to create a dense pattern of avoided crossings from which the resonance potential as well as a width function can be constructed.[36]

In order to handle large molecular basis sets and configuration spaces, it is mandatory to avoid complete diagonalization of the Q space and instead use standard codes for direct CI techniques. For efficient convergence, it is then desirable to avoid near degeneracies and to limit the number of roots below the resonance state under investigation. In the case of core-excited resonance states, as those deriving from metastable states of noble gas atoms, it is rather simple to isolate the resonance root from quasicontinuum ones by projecting out configurations of target-type occupancy.[14] (In the following, we use ''target'' in the sense of electron scattering as denoting the exit channel system, here AB^+.) In this respect, it is important to note that an accurate description of the target is not required for the construction of Q and, as already pointed out by Lypsky and Russek,[37] it is not neces-

sary to exclude whole classes of configurations such as antisymmetrized products of a Hartree–Fock (HF) target wave function with any of the unoccupied MOs. The only purpose of the projection is to cut a window into the spectrum of the quasicontinuum states in order to isolate the resonance. The size of the window depends on the variation of the respective resonance state with internuclear separation and the strength of its interaction with the continuum. Configurations describing the target ion plus a compact wave packet with energies below and above the window are then appropriately considered a part of the correlation space of the resonance state. The definition of the projectors P and Q in terms of electron configurations, thus, turns out to be rather obvious for core-excited resonances, in particular if the target can be rather well approximated by a one-determinantal HF wave function. It has to be noted, however, that just in these cases the optimal (HF) orbitals may be quite different for the resonance and target structure, respectively, due to significant orbital relaxation effects (e.g., upon excitation the 1s orbital of He contracts from 1.7 to 2.0 yielding a relaxation energy of 1 eV). The flexibility in the definition in P and Q is, therefore, welcome to circumvent disadvantages from a slowly convergent configuration expansion in nonoptimal orbitals: As long as properties are considered that pertain to one subspace only, such as the potentials V_* and V_+, different projections based on different sets of orbitals are allowed. Since the accuracy of the potential is really crucial, we propose such a projection scheme and call the procedure based on orbitals optimized for core-excited structures the ''resonance procedure'' and that based on optimal target orbitals the ''target procedure.'' For the calculation of the coupling elements $V_{\epsilon l}$ connecting the P and Q subspaces, common restrictions in *ab initio* programs confine us to a single set of orthonormal orbitals. Since, in this context, a simple description of the target is quite essential, we use the target procedure and try to account for relaxation in the resonance state by an extended MR-CI ansatz.

B. Coupling matrix elements $V_{\epsilon l}$ and width

1. Definition of the ''Penning MO''

The basic quantities for further analysis and calculation of the relevant cross section are the coupling matrix elements $V_{\epsilon l}(R)$, given by Eq. (29). One of the notorious problems in evaluating these quantities is connected with the combination of bound and continuum wave functions in $V_{\epsilon l}$. On the one hand, for an accurate treatment of the resonance structure ϕ_*, as well as the target structure Φ_+, one needs to employ quantum chemical methods that are based on L^2 basis functions and orbitals. On the other hand, the l decomposition and the phases of $V_{\epsilon l}$ depend critically on the long-range behavior of the continuum orbital $\varphi_{\epsilon l}$ attached to Φ_+ and this cannot be properly treated within a L^2 basis, but generally requires numerical radial functions or exponential functions e^{ikr}/r, both of which are difficult to handle in exchange integrals with L^2 functions. In electron scattering codes, the introduction of a radius at which L^2 and continuum functions are matched, is the common way out of this problem. We have avoided the R-matrix technique by proceeding in the following steps:

(1) Φ_+ and, by virtue of the Feshbach projection, ϕ_* are bound states and are calculated by the direct multireference CI method within an L^2 (i.e., Gaussian) basis.

(2) By integration over N-1 electron coordinates, we obtain a one-electron function

$$\varphi_P(1)=\langle\Phi_+(2\ldots N)|H_{\rm el}|\phi_*(1\ldots N)\rangle_{2\ldots N}, \tag{45}$$

which is L^2 by nature of Φ_+ and ϕ_*. $\varphi_P^*\varphi_P$ comprises the distribution of electrons, which may be created in the autoionization process. We may call this function the Penning MO (PMO).

(3) The coupling matrix elements, Eq. (29), are then simply obtained by projecting φ_P onto the energy shell as defined by the space of the $\varphi_{\epsilon l}$, the wave functions of the ejected electron of energy ϵ (as given by the resonance condition) and angular momentum l. In the present implementation, these functions are derived in numerical form in the static-exchange approximation with the $\varphi_{\epsilon l}$ chosen orthogonal to all orbitals occupied in Φ_+. This projection then reduces to simple overlap integrals

$$V_{\epsilon l}=\langle\varphi_{\epsilon l}|\varphi_P\rangle, \quad \epsilon=\epsilon_v. \tag{46}$$

The static-exchange approximation is considered perfectly adequate for systems that eject electrons of several eV and for which the target is of closed-shell nature, such as in the rare-gas–alkali cases. The ''Penning MO'' contains all relevant information about the resonance state that is required for the calculation of electron spectra. Note that the formal definition (46) of the PMO is the same regardless which procedure, resonance or target, is used, but the latter is the adequate one in combination with the static-exchange approximation.

For use in the dynamics calculations with Eqs. (33)–(39), the *ab initio* calculated coupling matrix elements need to refer to a partial-wave expansion with respect to the center of mass as origin. However, as argued in the next section, it is advantageous to calculate them from a partial-wave expansion centered at the rare-gas atom. By comparing the partial-wave expansions related to two different centers separated by a distance d along the z axis, it is easily verified that the corresponding coupling matrix elements are related by

$$V_{\epsilon l'}(d)=\sum_l V_{\epsilon l}(0)\sum_\lambda i^\lambda(2\lambda+1)[(2l+1)(2^{l'}+1)]^{1/2} \times\begin{pmatrix} l & l' & \lambda \\ 0 & 0 & 0\end{pmatrix}^2 \frac{u_\lambda(kd)}{kd}, \tag{47}$$

where the $u_\lambda\,(kd)$ are the regular Ricatti–Bessel functions.[38] Of course, the total width Γ is not affected by this shift of the reference point.

2. Stieltjes imaging

In order to stay within quantum chemistry codes, the orbital φ_P is actually calculated from $N-$electron matrix elements as

$$\varphi_P = \Sigma_i |\varphi_i\rangle \langle \varphi_i \Phi_+ | H_{el} | \phi_* \rangle_N . \tag{48}$$

If the orbitals φ_i used in the CI calculations diagonalize the Fock operator pertaining to the ground state of AB^+, they provide a discretized representation of the continuum with corresponding electron energies and coupling matrix elements given by the coefficients in expansion (48). Squares of these matrix elements constitute a discretized representation of the (energy dependent) width function $\Gamma_\epsilon(R)$.

In addition to the procedure described above, we have calculated the width function by a variant of the Stieltjes imaging procedure. Following a suggestion by Hazi,[20] a moment analysis of the rather irregular discrete spectrum is avoided instead, for each internuclear separation R, the corresponding cumulative step function

$$I(\epsilon) = \sum_i^{\epsilon_i < \epsilon} |\langle \varphi_i \Phi_+ | H_{\rm el} | \phi_* \rangle|^2 \tag{49}$$

has been fitted by an analytical expression. We then obtain $\Gamma(R)$ from

$$\Gamma(R) = 2\pi \left. \frac{dI}{d\epsilon} \right|_{\epsilon = \epsilon_v(R)} . \tag{50}$$

The shift $\Delta(R)$ may be derived from

$$\Delta(R) = \mathscr{P} \int d\epsilon \, \frac{dI/d\epsilon}{\epsilon - \epsilon_v} = \mathscr{P} \int dI (\epsilon - \epsilon_v)^{-1}. \tag{51}$$

Since $I(\epsilon)$ follows an exponential shape for energies around the resonance and above, we found it very useful to transform $I(\epsilon)$ into a function of $x = \exp[-a(\epsilon - \epsilon_v)]$ and to fit $I'(x)$ by a low-degree polynomial. This transformation introduces an adequate weighting of the data obtained for a rather large energy range. Stieltjes imaging of this kind was also used in some of our previous work.[17,21,22]

3. Static exchange scattering calculations

In the static exchange approximation,[24] the wave function $\varphi_{\epsilon l}(\mathbf{r})$ describing a continuum electron with asymptotic angular momentum l ($m=0$ understood) in the field of the closed shell target is the solution of

$$(-\tfrac{1}{2}\Delta + V_{\rm s.ex.}(\mathbf{r}) - \epsilon)\, \varphi_{\epsilon l}(\mathbf{r}) = 0, \tag{52}$$

where, in the case of two atoms,

$$V_{\rm s.ex.} = -\frac{Z_A}{r_A} - \frac{Z_B}{r_B} + 2J - \hat{K}, \tag{53}$$

with

$$J(\mathbf{r}) = \sum_j \int d\mathbf{r}' |\varphi_j(\mathbf{r}')|^2 / |\mathbf{r} - \mathbf{r}'|, \tag{54}$$

and

$$\hat{K} \varphi_{\epsilon l}(\mathbf{r}) = \sum_j \varphi_j(\mathbf{r}) \int d\mathbf{r}' \, \varphi_j^*(\mathbf{r}') \varphi_{\epsilon l}(\mathbf{r}') / |\mathbf{r} - \mathbf{r}'|. \tag{55}$$

In Eqs. (54) and (55), the sum is the overall occupied target orbitals.

By the one-center partial-wave expansion as defined in Eq. (26), Eq. (52) is transformed to a set of coupled equations for radial components $f_{\epsilon l l'}(r)$, which are solved under the boundary conditions for energy-normalized continuum functions, e.g., Eq. (27) for Coulomb functions. As customary, Eqs. (52)–(55) are solved iteratively where J is obtained in numerical form from Eq. (54) but $\hat{K}$ is represented by its projection on the set of GTO basis functions used in the calculation of the Penning MO. Because the regions very close to the He core are most important for the resonance–continuum coupling, the best convergence was obtained when using He as the expansion center, in spite of the fact that the off-center proton creates a strong long-range potential. Twenty-five coupled angular momentum channels turned out to be sufficient to obtain well-converged results for the complex coupling matrix elements, Eq. (46). The coupling matrix elements are finally transformed to the center of mass via Eq. (47).

C. Application to atomic resonances

In order to test our procedures, we have investigated the $(1s2s^2)^2S$ resonances of Li and He^-, two three-electron atomic systems that closely resemble the collisional complex under consideration here: the He^- resonance involves the same open shell $1s$ He orbital, and Li represents the united atom limit of $He^*(2s^3S)$ + H. Both cases have been treated previously by various theoretical methods[39–45] and comparison can be made with precise measurements of the resonance energies[46–52] and, in the case of He^-, also with experimental data for the width.[46–49]

As pointed out by Davis and Chung,[45] the proper account of electron correlation is essential for accurate results for the widths of these ^2S atomic resonances. A basis of $13s,7p,3d$ Gaussian functions, comparable to that used for He*+H, appeared to give converged results, once sufficiently diffuse functions had been included (to describe properly the continuum and the correlation in the resonance state). The $1s$ core orbital has been defined in a self-consistent-field (SCF) calculation for two electrons with either parallel (resonance procedure) or antiparallel spins (target procedure). This orbital was kept frozen in the subsequent multiconfiguration (SCF) calculation of the reference wave functions that were optimized in the space of ten configurations constructed from the $1s$, $2s$, $3s$, and $2p$ atomic orbitals. The Q space was generated in MR–CI by all single and double substitutions from the reference configurations, excluding the P-space configurations of the type $(1s)^2 ns$. n was restricted to >3 in the case of Li, for which the basis supported two Rydberg-type bound states, while no such states exist for He. For tests of the Stieltjes procedure, the virtual orbitals have been required to diagonalize the Fock operator pertaining to the $(1s)^2$ core.

TABLE I. $^2S(1s\,2s^2)$ resonance states of Li and He^-.

Method	Ref.	Energy[a] (eV)	Width (meV)
Li			
Resonance procedure	This work	51.034	36.35
Target procedure	This work	51.035	35.08
Saddle-point complex rotation	45	51.012	36.85
Quasiprojection operator	39	51.000	42.3
Quasiprojection operator	40	51.049	40.3
Expt., electron spectroscopy	50	50.92 (01)	
Expt., electron spectroscopy	51	51.004 (015)	
Expt., beam–gas spectroscopy	52	50.97 (05)	
He^-			
Resonance procedure	This work	19.375	10.25
Target procedure	This work	19.382	11.22
Saddle-point complex rotation	45	19.376	11.56
Complex rotation	41	19.402	11.72
Quasiprojection operator	42	19.4	13.9
Close coupling	43	19.365	11.0
Variational	44	19.4	15.0
Expt., transmission	46	19.3	12.0
Expt., transmission	47	19.367 (009)	9 (1)
Expt., transmission	48	19.35 (02)	13.0
Expt., electron spectroscopy	49		11.0 (0.5)

[a]Relative to the ground-state energies of $-7.279\,913$ for Li^+ and $-2.903\,724$ for He.

The results of our calculations are collected in Table I, which also comprises the most reliable experimental and previous theoretical results. Both procedures, the resonance and target ones, are seen to lead to basically equivalent results. These compare favorably with other theoretical results and with experiments (see Ref. 45, and references therein). From the agreement observed for He and Li, we estimate that the resonance potential of He*+H, calculated in the same way, should be accurate to about 10 meV, and we expect an accuracy of the V_l of better than 5%.

The results for the widths given in Table I have been obtained from the static-exchange scattering calculations as described above. The corresponding Stieltjes widths are larger by only about 2% in the case of He^-, but by as much as 15% in the case of Li.

[In order to illustrate the importance of the $1s$ orbital relaxation, we note that the difference between the resonance energies obtained by the two procedures is as much as 0.04 hartree (1.09 eV) at the MC–SCF level.]

D. Heavy particle dynamics

The radial wave functions F_J^+ and F_J of Eqs. (22)–(24) are calculated by the Numerov–Cooley algorithm,[53] which is easily generalized to complex potentials. Integration over entrance and exit channel energies is, of course, done numerically. Even though the real part of the entrance channel potential supports a number of resonances, they are effectively suppressed by the imaginary part of the potential. Appreciable autoionization sets in only above the centrifugal barrier and its probability soon reaches a value that is only weakly dependent on E or J. For He*+H, this value is ~ 0.79. Only slightly above the barrier we observe a significant variation down to 0.6 or up to 1.0 over an energy range of about 5 meV, which reflects the familiar oscillating behavior of barrier transmission. The shape of this onset of autoionization is periodic with about four J quanta. To map out the onset region properly, about 60 energies are required, evenly spaced by $10^{-4}E_h$. Since the oscillations largely cancel in the sum over J, the electronic spectra are nevertheless nearly converged with only 20 energies spaced by $4\times 10^{-4}E_h$. The steep exit channel potential of HeH^+, on the other hand, supports many resonances up to $J<27$, the lower ones being rather narrow and quite prominent in the electron spectra. In order to avoid the cumbersome integration across resonances of strongly varying width, we have used the discretized (and normalized) continuum states as obtained by limiting the HeH^+ to a finite sphere (with a radius of about $80a_0$). Thus, bound states, resonances, and background continuum are all treated in the same way and, as completeness checks showed, integration across the bound state/continuum boundary, and the resonances as well, is very stable and trivial in this way. In particular, it was verified that the autoionization probability as calculated in the two channels did fully agree, i.e.,

$$\langle F_J|\Gamma|F_J\rangle=\sum_k \langle F_J|\Gamma^{1/2}|F^+_{J'}(E_{+k})\rangle\langle F^+_{J'}(E_{+k})|\Gamma^{1/2}|F_J\rangle. \tag{56}$$

By limiting this sum to $E_{+k}\leqslant E$, the rhs turned out to be reduced only insignificantly. This proves the validity of one of the requirements for the local approximation of the complex potential, the sufficient completeness of the accesible exit channel vibrational states, as discussed in Sec. II A.

The main computational effort goes into calculating the matrix elements $\langle F^+_{J'}|V_l|F_J\rangle$, the number of which runs into millions. Efficiency could be enhanced by integration with a wider grid than that used for the Numerov algorithm and by an expansion of the V_l in terms of piecewise polynomials.

IV. POTENTIALS AND COUPLING ELEMENTS FOR He*(2^3S)+H

The methods described above have so far been applied to the autoionizing systems $He(1s2s^3S)+H,D,Li$. The main results for the collision systems involving H and D have already been published in comparison with high-resolution electron spectometric experiments.[25] Here, we restrict ourselves to the most fundamental of these collision processes, but we give a description of computational details for this case and a thorough analysis of the resulting spectra.

A. Electronic structures

The asymptotic $He(1s2s^3S)+H(1s)$ states split at finite internuclear distances into $^2\Sigma$ and $^4\Sigma$ states. The exit channel electronic states of the HeH^+ system are singlet states, so that only doublet $^2\Sigma^+$ states of He*H are autoionizing. The

TABLE II. Exponents of the GTO basis set for He+H.

l	He	H
s	10s set of Ref. 54	First 6 of the 10s set of Ref. 54
	0.04, 0.016, 0.0064	0.55, 0.24, 0.10, 0.05, 0.025
p	3.0, 0.9, 0.3, 0.1, 0.04, 0.016	1.2, 0.3, 0.1, 0.04
d	0.12, 0.04	0.6, 0.18

electronic structure of the resonance states undergoes significant changes as the interatomic distance varies. The lowest resonance state, i.e., that correlated to the He($2s^3S$) + H asymptote, is at short interatomic distances well described by the single configuration $1s(2\sigma)^2$, where the orbital 2σ is dominated by a H^- 1s component. At intermediate distances, the configurations $1s(3\sigma)^2$ and $1s(2\sigma 3\sigma)$ with an antibonding delocalized 3σ orbital gain significant weight. At large separations, the asymptotic state is finally described by these three configurations with relative weights 3:3:2. Due to the large polarizability of He*, at intermediate ranges there are also significant admixtures by the He $2p_\sigma$ orbital; in particular for the state correlating to He($2s^1S$).

In our calculations, we started from MC–SCF wave functions optimized in the space of the 14 $^2\Sigma^+$ configurations that are possible from the six ''active orbitals'' $1s,2\sigma - 4\sigma,1\pi_x,1\pi_y$ under the condition that 1s is at least singly occupied. This ansatz provides an adequate description of the four asymptotes correlating to He* $^{1,3}S$ and $^{1,3}P$, respectively. The orbitals are determined to minimize the energy average of the two lower resonance states so that the 1s orbital optimally describes the unpaired He K-shell electron. Virtually identical orbitals resulted from a somewhat simpler procedure by which the 1s orbital was derived from a preceding SCF step for either the $1s2\sigma 3\sigma\ ^4\Sigma$ state or the $1s2\sigma\ ^3\Sigma$ ionic state, respectively, and then freezing the 1s orbital in the MC–SCF step. We note that this choice for the 1s orbital is in contrast to previous theoretical work,[14,27] in which SCF orbitals from HeH^+ have been used, i.e., a 1s optimized for double occupancy.

The Q space for the final CI was generated by all single and double substitutions from the 14 reference configurations, excluding the configurations of the type $(1s)^2 n\sigma$ with $n>4$. For $n\leqslant 4$, the latter configurations correlate to the lowest excited (Rydberg) states He+H* and are not part of the exit channel asymptotically. As it turned out, they do not contribute much to the resonance states either, but they are necessary to account for lower roots of the variational CI, which prevent the resonance from being too low in energy. Their inclusion in Q space, therefore, reduces the shift $\Delta(R)$.

B. Basis set and separated atom properties

Table II shows the Gaussian basis set used in our final calculations of the He*($2s^3S$)+H potential, in which we have also obtained the potentials that correspond to the asymptotes He*($2s^1S,^{1,3}P$)+H. Table III gives some atomic properties for He and H as calculated from the basis set given in Table II. The He* $^{1,3}S$ excitation energies are seen to be correct to within 0.000 25 E_h, thus, reproducing their difference to three significant figures. Dipole polarizabilities agree to within 1% with the theoretical values of Victor *et al.*,[56] indicating that our long-range potentials should be quite reliable. The C_6 coefficient is indeed in excellent agreement with the most recent value,[60] while C_8 is still fairly good. It differs by 1% from the result of Proctor and Stwalley,[59] and reproduces 88% of the most reliable value.[60]

TABLE III. Pertinent properties of separated atoms (in atomic units).

	State	Property	This work	Other	Ref.
He	$1\ ^1S$	E	−2.899 98	−2.903 72	55
		α_1	1.373	1.382	56
	$2\ ^3S$	ΔE	0.724 83	0.728 49	55
		α_1	314.6	316.2	56
	$2\ ^1S$	ΔE	0.754 01	0.757 75	55
		α_1	791.2	802.3	56
	$2\ ^3P$	ΔE	0.767 18	0.770 56	57
	$2\ ^1P$	ΔE	0.776 86	0.776 14	57
H	$1\ ^2S$	E	−0.499 99	−0.5	
		α_1	4.498 70	4.5	
		EA	0.027	0.027	55
He*−H	$^3\Sigma$	C_6	−87.76	−88.2	58
				−86.64	59
				−87.84	60
		C_8	−4554.0	−4593.0	59
				−5181.0	60
		C_{10}		−41650	60

C. Potentials

The four $^2\Sigma^+$ potentials for He*+H as calculated by the resonance procedure are given in Table IV. They are also shown in Fig. 1, where our He*(2^3S)+H$^2\Sigma^+$ potential is compared to those calculated previously.[27,14] The well depth of our potential, $D_e=2.28$ eV, agrees very well with the empirical value $D_e=2.26$ eV determined by Morgner and Niehaus from their PI spectra,[61] and may be compared with older *ab initio* results of $D_e=1.91$ eV and $D_e=2.07$ eV, obtained by Miller and Schaefer[27] and Hickman *et al.*,[14] respectively. The improvement is due to larger orbital and CI spaces used here (5792 configurations). These spaces have been restricted in the older calculations in order to allow for a full diagonalization of the Hamiltonian matrix used in ''golden-rule'' or Siegert-type calculations for Γ.[27,28] As compared to the empirical potential,[61] ours is significantly more attractive at distances larger than R_e since the latter was adjusted to the long-range potential calculated in Ref. 27, which missed a significant part of the van der Waals attraction due to basis set limitations. The well depth of the potential derived from R-matrix calculations by Sarpal[30] is 0.19 eV larger than ours.

A preliminary version of our potential, which is virtually identical with the one presented here, has been used by

TABLE IV. $^2\Sigma^+$ potentials of He*H. Energies in μE_h relative to the $\mathrm{He}(2^3S)+\mathrm{H}(1^2S)$ asymptote.

R (a_0)	$\mathrm{He}(^3S)+\mathrm{H}$	$\mathrm{He}(^1S)+\mathrm{H}$	$\mathrm{He}(^3P)+\mathrm{H}$	$\mathrm{He}(^1P)+\mathrm{H}$
1.60	190 339			
1.70	143 109			
1.80	102 920			
1.90	68 801			
2.00	39 927	144 260	218 910	247 230
2.10	15 589			
2.25	−13 735	101 340	170 170	184 920
2.50	−47 562	73 550	132 140	146 640
2.75	−67 752			
3.00	−78 480	43 880	73 920	113 810
3.25	−83 196			
3.50	−83 779	30 270	46 800	100 590
3.75	−81 645			
4.00	−77 768	22 000	37 200	92 640
4.25	−72 816			
4.50	−67 249			
4.75	−61 384			
5.00	−55 438	15 090	33 860	77 230
6.00	−33 214	13 780	33 460	64 000
7.00	−16 150	14 780	32 930	56 320
8.00	−6 079	18 920	32 560	52 500
9.00	−2 038	24 970	33 220	50 790
10.00	−712	28 320	36 270	50 370
11.00	−267	29 110	39 590	50 820
12.00	−108	29 310	41 270	51 430
15.00	−12	29 420	42 270	51 970
Inf	0	29 440	42 350	52 030

Waibel *et al.*[15] in an analysis of the first electron spectra obtained with high resolution. They were able to reproduce the low-energy onset of the spectrum quite accurately in model quantum calculations with an empirical fit of the width function. They concluded that the calculated well depth should be correct to within about 20 meV, the lower limit of energy resolution achieved in their experiment. Our final potential has a well that is 8 meV deeper and is, thus, also within the experimental uncertainty. The well depth obtained by the target procedure, however, is about 25 meV smaller than the one obtained by the resonance procedure and falls slightly outside the experimental error.

For the $\mathrm{He}^*(2s^1S)+\mathrm{H}\ ^2\Sigma^+$ potential we have obtained a well depth of $D_e=0.43$ eV, while Miller and Schaefer[27] derived $D_e=0.39$ eV. As to the equilibrium distances, their result is larger for the ^3S curve as expected from the missing attraction, but somewhat surprisingly, it is shorter for the ^1S curve. The parameters for the potential wells of the two lowest resonance states are collected in Table V.

The peculiar shape of the $\mathrm{He}^*(2s^3P)+\mathrm{H}\ ^2\Sigma^+$ potential is due to an avoided crossing with the lower $\mathrm{He}^*(2s^1S)+\mathrm{H}\ ^2\Sigma^+$ potential as discussed previously.[27] The shoulder in the $\mathrm{He}^*(2s^1P)+\mathrm{H}\ ^2\Sigma^+$ potential reflects an avoided crossing with the $^2\Sigma^+$ potential asymptotically corresponding to $\mathrm{He}^+ + \mathrm{H}^-$. Qualitatively, the same behavior was obtained by Paidarova *et al.*[62] in their atoms-in-molecules calculations for the diatomics-in-molecules model of PI of H_2 by He*.

In order to illustrate the significant contribution due to the ionic structure $\mathrm{He}^+ + \mathrm{H}^-$, we have included in Fig. 1 the ionic potential $-1/R-\alpha(\mathrm{H}^-)/2R^4$ (dashed-line). At the equilibrium of the resonance state, its dipole moment amounts to about 3 a.u., nearly compatible with a transfer of one electron. The analysis of the dipole moment curves also reveals that there is a further avoided crossing of the states correlating to He* ^1S and ^3P around $3.5a_0$.

Our $\mathrm{He}(1s^2)+\mathrm{H}^+$ potential agrees with the one due to Bishop and Cheung[63] and Kolos and Peek[64] to better than 3 meV at all distances reported, but we have added some further short-range points as required for the collision process under investigation.

D. Coupling elements and width function

As described in Sec. III B 1, the energy-dependent coupling with the continuum is represented in the form of a compact (L^2) ''Penning MO'' without phase information being lost. This MO is projected onto the states of the continuum electron in the exit channel, which are calculated within the static-exchange approximation for up to 25 coupled angular momentum channels. For $R=1.6$, 2.0, 3.0, and $5.0a_0$, we have tested the convergence by gradually changing the number of coupled channels from 12 to 25. The

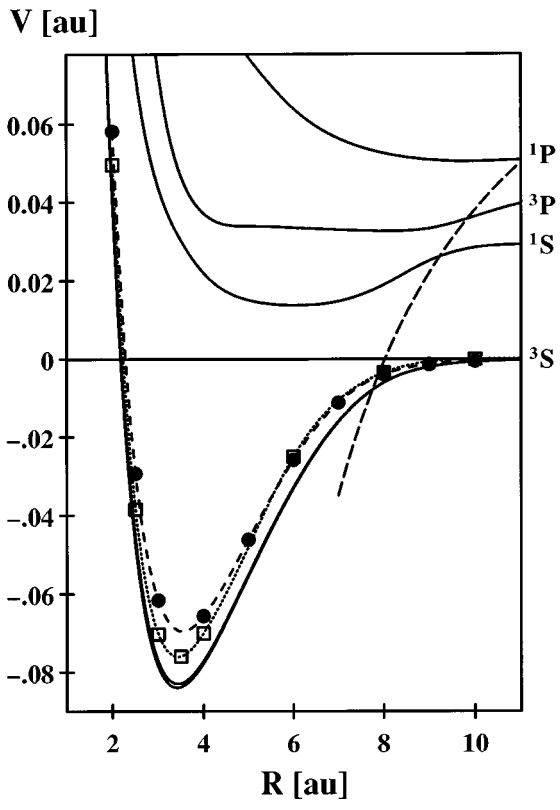

FIG. 1. Calculated potential energy curves of the lower $^2\Sigma$ resonance states of He*+H. The labels denote the asymptotic He* states. Also shown are previous *ab initio* potentials from Ref. 27 (dotted line) and Ref. 14 (dashed line). The position of the ionic structure $\mathrm{He}^+\mathrm{H}^-$, responsible for a sequence of avoided crossings, is indicated by the long-dashed line.

TABLE V. Parameters for the potential wells of the two lowest resonance states of He-H.

Asymptote	D_e (eV)	$R_e(a_0)$	Method	Ref.
$2\ ^3S$	2.284	3.42	MR–CI	Present
	2.26	3.3	Empirical	61
	1.91	3.52	CI	27
	2.07	3.5	CI	14
	2.47	3.39	R matrix	30
$2\ ^1S$	0.426	6.05	MR–CI	Present
	0.39	5.78	CI	27

convergence was smooth in all four cases. In order to converge the four leading l components to four significant figures, 17 channels for $R=1.6a_0$ and 22 channels for $R=2.0a_0$ were sufficient.

The resulting complex l-dependent coupling matrix elements are listed in Table VI and shown in Fig. 2 for a set of internuclear separations. The characteristic spiral curves are the consequence of a strong decrease of the norms with increasing internuclear separation (as expected from the exchange mechanism) and phase changes that are partly due to the related energy changes. For short distances (including the turning point region), the $l=2$ coupling is dominant. Further out, the isotropic component $l=0$ is the largest, but significant couplings exist for l up to 4. Note that this angular decomposition refers to the center of mass (c.m.), as required for the heavy-particle dynamics. There appears to be little resemblance to the other coupling elements available in the literature.[13,14] They have been obtained by a partial wave expansion in terms of Coulomb waves centered on H^+. We have performed an additional calculation assuming a pure Coulomb wave function for the continuum electron with the result that the $l=1$ c.m. partial wave predominates at shorter internuclear separations. This demonstrates that the perturbation due to the ground-state He atom influences significantly the phase shifts and the general behavior of the complex coupling elements.

The partial widths $\Gamma_l=2\pi|V_l|^2$ are shown in Fig. 3, together with the total width. Here, the changing weights of different l waves is clearly seen. The partial-wave components with $l=0$ and 2 (s and d waves in the c.m. coordinate system) are dominant up to $4a_0$, the $l=2$ component being the leading one up to $2.75a_0$. From around $4a_0$, the $l=3$ component mixes in significantly. The $l=1$ component stays suppressed until the asymptotic region is reached ($R>6a_0$).

The l distribution of the coupling matrix elements suggests a significant angular momentum exchange in this system, dominated by $|\Delta J|=2$ at shorter distances. A classical estimate based on recoil arguments led Waibel *et al.*[15] to the conclusion that $|\Delta J|<1$, supporting the idea of negligible angular momentum exchange. In this pure recoil model, the emitted electron is considered as being emitted isotropically from the He core and the interaction of the escaping electron with the Coulomb center is neglected. This may be adequate for a system such as He*+Li, where the entrance channel turning point is rather large ($\sim 4a_0$) and the center of mass

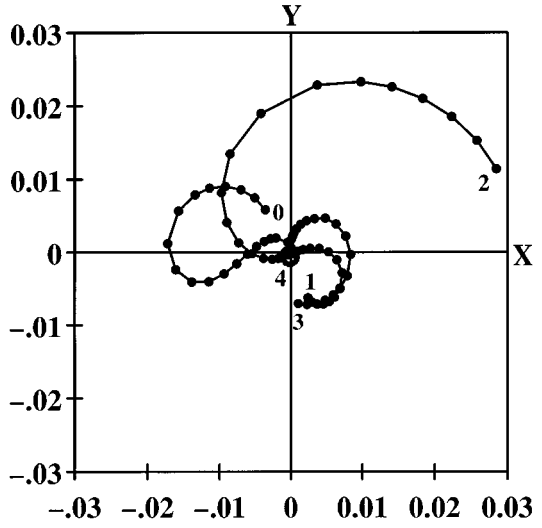

FIG. 2. Complex coupling elements $V_l(R)$ (in a.u.). The internuclear distances indicated by points are those of Table VI, starting with the shortest one at the point labeled by l. Note that the most efficient region for ionization in thermal collisions involves the points 6–9.

is close to Li^+. The estimated angular momentum transfer of about $l=4$ is, indeed, in agreement with our calculations. For He*+H, on the contrary, the turning point is only $2.1a_0$, so that there is a large anisotropy of the Penning MO in the vicinity of the He core, and in addition, the center of mass is much farther away from the Coulomb center.

Figure 4 compares the total width functions obtained from the PMOs of the target and resonance procedures, respectively, with those from the Stieltjes procedure. For further comparison, two previously calculated total widths[13,14] are also included. The differences among the width functions obtained in the present investigation are on average within 10%. The R-matrix width function agrees also within this margin with ours in the region between 3 and $5a_0$ but is 20% higher around the maximum and decays more slowly for larger distances.[30] Our total widths are similar in shape to the earlier result of Hickman *et al.*,[14] but the absolute values are lower by a factor of about 2. For completeness, we note that the semiempirical fit of Waibel *et al.*[15] deviates significantly in shape, especially in the transition region of intermediate internuclear separations and in the long-range behavior. This is probably due to the fact that the fit was based on the approximate treatment by Eq. (43).

We have also analyzed the dependence of the width function on the electron energy for several fixed internuclear separations. As already mentioned in Sec. III A, the well-defined quantity is the sum $V_*+\Delta$, while V_* and Δ are only intermediate quantities depending on the choice of the P and Q projectors. The shift Δ is related to the energy-dependent width function by Eq. (18). It means that the shape of the width function also depends on the definition of the P and Q operators. On the other hand, the value of the width function for electron energies close to the resonance energy should stay stable, independent of the particular choice of P and Q. In Fig. 5, the normalized width functions obtained

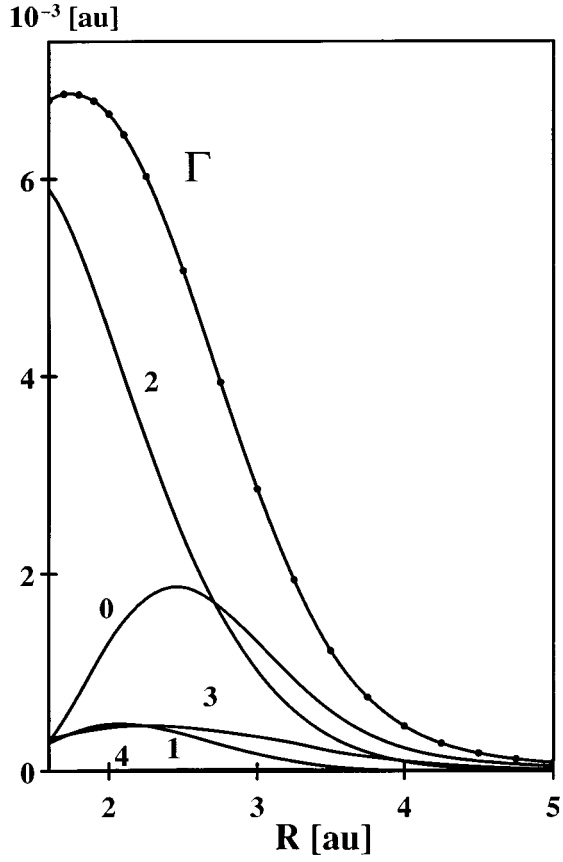

FIG. 3. Partial width functions $\Gamma_l = 2\pi |V_l(R)|^2$ for $l = 0-4$ and total width $\Gamma = \Sigma_l \Gamma_l$.

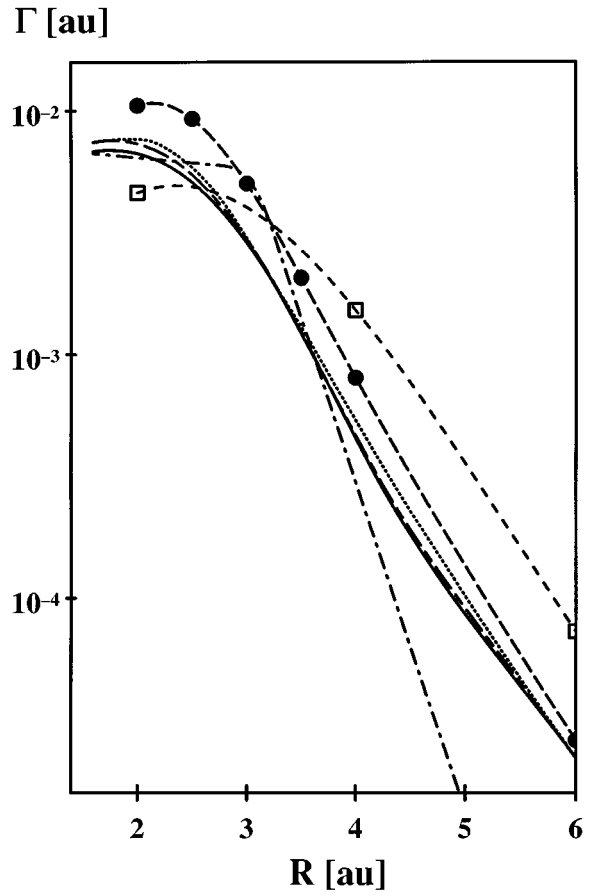

FIG. 4. Comparison of width functions. Solid line: ''target'' PMO projected on continuum functions. Short/long dashed line: ''resonance'' PMO projected on continuum functions. Dotted line: from the Stieltjes imaging procedure. Short dashed: Ref. 13; long dashed: Ref. 14. Dotted/dashed line: best fit function of Ref. 15.

in target (solid line) and resonance procedures (dashed line) are compared for three different internuclear separations. The curves are smooth and pairs of curves corresponding to the same R indeed cross at the resonance energy, giving the same $\Gamma(R)$. Around the resonance energy, the width function obtained in the target procedure changes less than the corresponding one from the resonance procedure, indicating that the former may be more consistent with the local potential approximation than the latter. We have incorporated the energy derivative $\partial\Gamma_e(R)/\partial\epsilon$ in test calculations of electron spectra as a first correction to the local approximation but found only negligible changes, in agreement with Morgner's[12] conclusions about the validity of the local approximation.

E. Internal angular distribution

Experimental data for the angular dependence of the electron spectra for repulsive systems have often been analyzed in terms of the so-called internal angular distribution,[65,31] i.e., the angle-dependent intensity of the emitted electron in the frame of the collisional complex, Eq. (30). This distribution is intrinsically unmeasurable,[2] but could be used in the classical description of the angular distribution of ejected electrons. With the help of the approximate Eq. (42), the observed angular dependence can be used to determine α_l and derive some information on the internal angular distribution. Merz *et al.*[23] have concluded from an inspection of the AI part of the spectrum that the internal angular distribution exhibits similar maxima in the backward as well as in the forward direction. Furthermore, both maxima apparently exceed the minimum around $\theta = 90°$ by at least a factor of 2–3. We have calculated $P_{\rm int}$ without any approximation. Figure 6(a) shows the *ab initio* internal angular distribution for several internuclear separations R, as obtained from Eq. (30) using V_l from Table VI. There is considerable anisotropy and asymmetry present. For short distances, which mainly contribute to the associative part of the spectrum, there are sharp maxima both in the forward as well as in the backward direction, and a smaller one near the perpendicular direction. For $R > 3.0a_0$, the forward maximum starts to be larger then the backward one.

For comparison, Fig. 6(b) displays the internal angular distribution as obtained by approximating the continuum electron wave function simply by a pure Coulomb wave. The difference from Fig. 6(a) demonstrates the inadequacy of a Coulomb wave approximation even for a qualitative description of the internal angular distribution. This approximation implies that the angular momentum channels stay decoupled

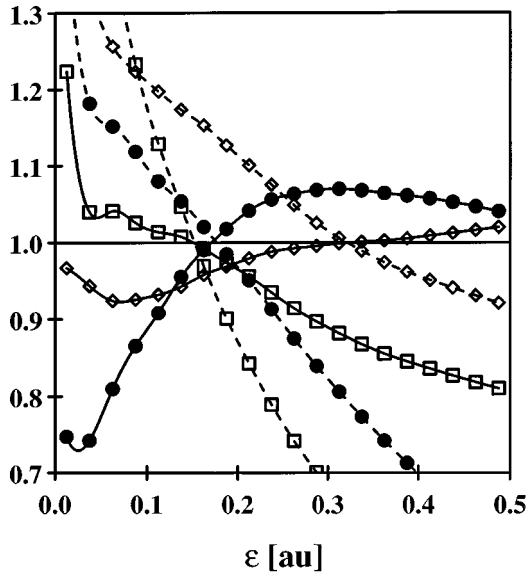

FIG. 5. Reduced width $\Gamma_\epsilon(R)/\Gamma_{\epsilon_v}(R)$ as a function of ϵ for $R=2$ (◇) $R=3.5$, (□), and $R=5$ (○), respectively. Solid lines: Γ from target PMO, dashed lines: Γ from resonance PMO.

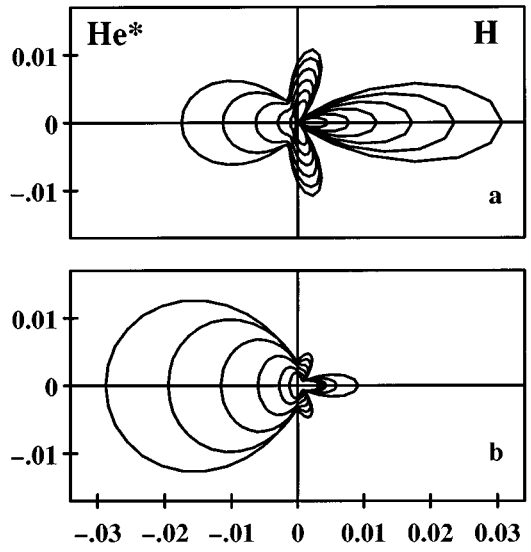

FIG. 6. Internal angular distribution $P_{\rm int}(\theta,R)$ of the electrons ejected from the collision complex He*$(2\,^3S)$+H. The parameter R is varied in steps of $\Delta R=0.25a_0$, starting at $R=2.25a_0$ (outer curve) to $R=3.5a_0$ (inner curve). The intensity scale of the polar plot is proportional to the autoionization width $\Gamma(R)/2\pi$ (a.u.). (a) From coupling elements due to projection on static-exchange continuum functions. (b) From coupling elements due to projection on (inappropriate) pure coulomb functions centered at H.

even at short range and neglects the phase changes due to the He core. Still, it appears to give an acceptable total width $\Gamma(R)$, which demonstrates that the latter is insensitive to l decomposition.[13,14]

F. Entrance channel related properties

We have calculated angle–differential cross sections for elastic scattering, Eq. (41), using the entrance channel complex potential with and without its imaginary part $i\Gamma/2$. Both results are averaged over the velocity distributions discussed later on and the results are compared in Fig. 7. The oscillations dominating the scattering pattern between forward and backward glory are ''diffraction oscillations'' typical for collisions of light atoms. For low collision energies, when orbiting is possible, they are usually interpreted as due to the interference between directly scattered waves and surface waves. For $J>27$, the rotational barrier starts to be higher than the mean relative velocity, and only for lower J there is appreciable probability for autoionization, which induces the differences between the two cross sections. Still, the global effect is an overall damping with the main difference in the shapes being that two peaks at 45° and 155° are somewhat more pronounced. Therefore, the measurement of the elastic scattering angular differential cross section is not a sensitive probe of the width function $\Gamma(R)$.

We have also analyzed the J and collision-energy dependence of partial contributions to the total ionization cross section. Figure 8 shows the (energy-averaged) J dependence of partial cross sections $\langle\sigma_J\rangle$, $(\sigma=\Sigma_J\sigma_J)$. The opacity function $\langle O_J(E)\rangle$ is also displayed. In spite of energy averaging, the partial cross sections (as well as the opacity function) oscillates as a function of entrance channel angular quantum number J. The general behavior is as expected for attractive Penning systems and low-energy collisions: as long as the collision energy $E_{\rm rel}$ is sufficiently small in comparison to the potential well depth D_e, the opacities $\langle O_J(E)\rangle$ are almost constant for all $J<J_{\max}$ and for $J>J_{\max}$ they are close to zero. Our energy-averaged opacity function has a constant value 0.79 for $J<15$, falls off to half that value for $J=27$ (which is $J_{\max}$ for the mean relative velocity), and for $J>40$, it is practically zero.

As we have recently discussed,[21] for attractive Penning systems $(D_e\gg E_{\rm rel})$, the collision energy dependence of the cross sections is mainly due to the variation of the number of heavy particle partial waves that surmount the rotational barrier $[0<J<J_{\max}(E_{\rm rel})]$ and access short distances with a large width, thus effectively contributing to ionization. Figure 9 shows the autoionization probability $P_J(E_{\rm rel})$ as a function of collision energy for specific angular momenta. For given J there is a characteristic near-threshold resonant behavior and the pattern repeats for groups of four successive J. So, for example, the autoionization probability shows a pronounced maximum $(J=19)$, broad maximum $(J=20)$, smooth monotonic rise up $(J=21)$, and maximum followed by minimum $(J=22)$.

We have calculated the energy-dependent total ionization cross section, as well as the associative ionization cross section, and the cross section for long-lived resonance states. The results are presented in Fig. 10 together with some previous results for comparison. The oscillations in the calculated total ionization cross section (the counterpart of glory oscillations and orbiting resonances in the energy dependence of elastic scattering) are clearly seen. In order to reproduce the oscillations, we have used a dense energy grid (step=0.0001 a.u.). Contrary to the previous calculations,[15]

TABLE VI. Electronic coupling matrix elements $V_l = x_l + iy_l$, Eq. (38), and width Γ, Eq. (17) (1×10^{-6} a.u.).

	$l=0$		$l=1$		$l=2$		$l=3$		$l=4$		$l=5$		
R (a_0)	x_0	y_0	x_1	y_1	x_2	y_2	x_3	y_3	x_4	y_4	x_5	y_5	Γ
1.60	−3593	5856	2385	−6227	28 457	11 403	1036	−7028	−381	563	96	−82	6801
1.70	−5078	7479	2948	−6816	25 789	15 278	2270	−7174	−539	507	104	−63	6865
1.80	−6997	8576	3694	−7116	22 351	18 512	3545	−7020	−718	408	112	−37	6859
1.90	−9180	9047	4547	−7102	18 365	20 981	4797	−6559	−891	264	115	−5	6796
2.00	−11 404	8797	5382	−6769	14 107	22 565	5927	−5847	−1041	76	115	31	6665
2.10	−13 402	7905	6085	−6184	9801	23 259	6868	−4914	−1150	−142	107	68	6453
2.25	−15 708	5688	6862	−4987	3701	22 820	7878	−3240	−1221	−495	86	123	6031
2.50	−17 207	1208	7175	−2796	−4204	18 974	8354	−304	−1099	−1056	28	194	5069
2.75	−16 091	−2372	6431	−1019	−8538	13 478	7652	2213	−763	−1456	−47	235	3944
3.00	−13 848	−4068	5244	58	−9743	8179	6311	3884	−332	−1644	−120	241	2862
3.25	−11 488	−4026	3964	503	−8972	4097	4802	4682	74	−1649	−183	220	1943
3.50	−9 368	−2953	2677	526	−7328	1308	3298	4618	343	−1485	−223	181	1219
3.75	−7598	−1566	1689	370	−5486	−190	2180	4337	580	−1300	−265	127	748
4.00	−6092	−252	932	139	−3866	−829	1366	3841	728	−1098	−301	70	453
4.25	−4813	791	381	−81	−2617	−952	815	3266	800	−908	−327	19	280
4.50	−3745	1474	−5	−240	−1741	−836	450	2715	821	−740	−342	−22	182
4.75	−2840	1851	−251	−330	−1159	618	227	2224	806	−600	−344	−52	123
5.00	−2109	1964	−405	−361	−793	−398	82	1814	772	−484	−337	−73	86
6.00	−468	1380	−485	−202	−362	166	−99	807	557	−192	−247	−95	23
7.00	6	647	−335	33	−311	274	−99	335	305	−13	−116	−92	5.9
8.00	90	249	−165	134	−192	188	−53	131	107	42	−15	−57	1.4
9.00	59	83	−56	97	−79	93	−24	55	29	28	13	−22	0.2
10.00	28	25	−13	47	−27	40	−10	24	9	13	10	−6	0.05

the transition from low-energy to high-energy behavior is smooth. Model calculations[21] using four different versions of the width function $\Gamma(R)$ have resulted in total ionization cross sections that varied by less than 10%, even though the corresponding (angle-integrated) electron energy spectra were quite different in shape. Available experimental data for the total ionization cross section with their typical uncertainties of 20%–30% are not sufficiently accurate to provide a significant test of the width function. The recommended data for the total ionization cross section, compiled from various experiments,[67] start to deviate from our theoretical curve for collision energies $E_{\mathrm{rel}}>30$ meV, and are 35% lower around $E_{\mathrm{rel}}=1$ eV. On the other hand, the recommended data for the associative ionization cross section are in reasonable agreement with our calculations.

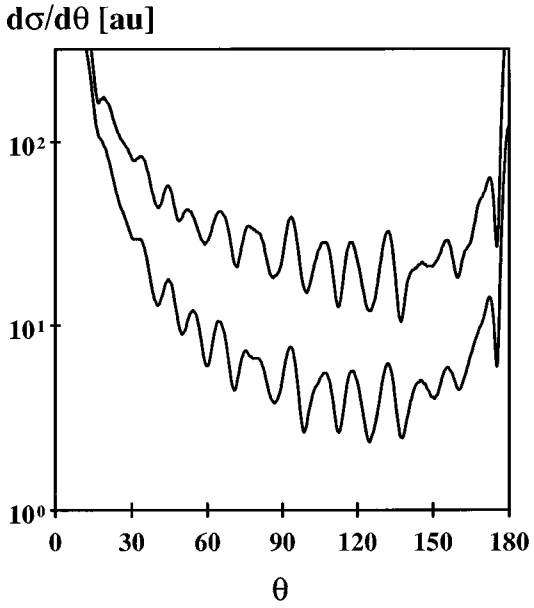

FIG. 7. Elastic differential cross section. Upper curve: including only the real part of the potential, i.e., $\Gamma=0$. Lower curve: including also the calculated imaginary part, $i\Gamma/2$.

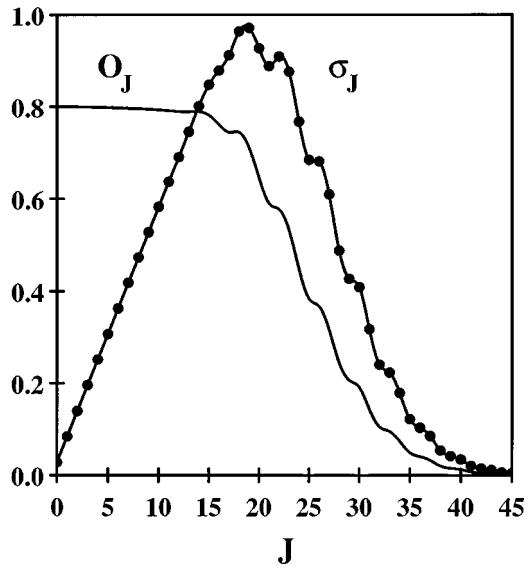

FIG. 8. Collision energy averaged opacity function for autoionization $\langle O_J(E)\rangle$ (solid line) and partial autoionization contributions σ_J scaled by 0.04 (solid line with dots)

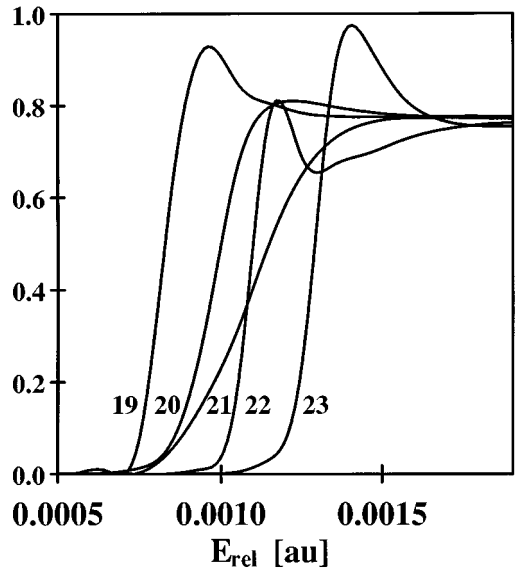

FIG. 9. Autoionization probabilities $P_J(E_{\rm rel})$ as a function of collision energy for specific angular momenta J.

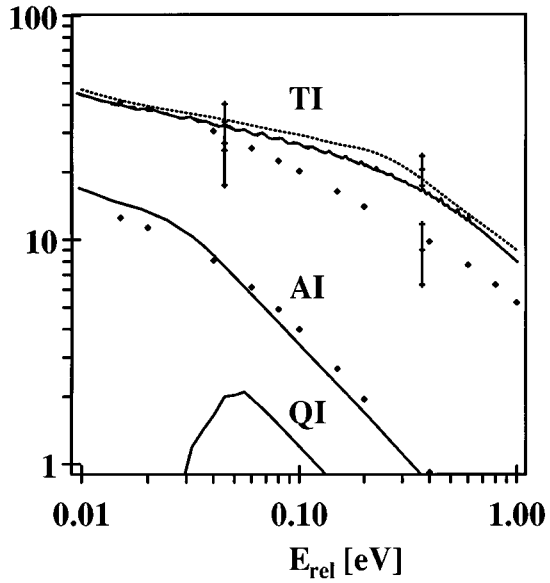

FIG. 10. Total ionization cross section (TI) as well as associative ionization cross section (AI) and cross section for long-lived resonance states (QI), versus collision energy. Solid line, present calculation; dashed line, Ref. 15, and ◇, recommended values from Ref. 67, measurements, Ref. 61 and references in Ref. 15.

The computed total ionization cross section, averaged over the velocity distributions of two perpendicular beams of H and He*, with a mean relative collision energy of $\langle E_{\rm rel}\rangle = 50$ meV, is $114.7a_0^2$. This may be compared with the value of $111.6a_0^2$ obtained for the single collision energy $E_{\rm rel} = 50$ meV. The experimental value deduced by Morgner and Niehaus[61] is $(120 \pm 20)a_0^2$.

Figure 11 shows the energy-averaged local autoionization rate

$$P(R) = \int \Gamma(R) \sum_J |F_J(E,R)|^2 f(E)\,dE, \tag{57}$$

together with the (arbitrarily scaled) width function $\Gamma(R)$. $P(R)$, being modulated by the square of the entrance channel wave function, resembles on average the shape of $\Gamma(R)$ for $R > 2.5a_0$, has a sharp maximum at 2.38, and falls steeply to zero at about $2a_0$. Fast oscillations of the local ionization rate are clearly visible. One of the findings of the model calculations mentioned above was that the associative part of the spectrum with the complex rovibrational structure is almost independent of the shape of $\Gamma(R)$, whereas the Penning part of the spectrum is substantially more sensitive to it. In the semiclassical sense, the AI part of the spectrum is of the ''reflection'' type,[68] i.e., the difference potential maps the radial distribution around the turning points $R_t(J)$ of the entrance channel motion in to the electron spectra. The local value $\Gamma(R_t)$ appears then as a simple scaling factor. For $E_{\rm rel} = 50$ meV, the turning point varies only from 2.17 to 2.42 for J values between 0 and 26, respectively. It is clear then that the AI spectra are not very sensitive to the shape of $\Gamma(R)$ in the small region around the maximum of $P(R)$. Figure 11 shows that the saturation of our width function occurs in the classically forbidden region. Therefore, it cannot be probed by measurements at low collision energies.

V. ELECTRON SPECTRA FOR He(^3S) + H

A. General structure of the spectra

Intensive studies in a variety of cell and molecular beam experiments have furnished energy-dependent total and associative ionization cross sections,[69] as well as ion[23] and electron energy spectra.[15,23,61] The most detailed information on the ionization mechanism can be extracted from electron spectrometry. A series of beautiful measurements by Hotop and co-workers[15–17,21–23] has recently culminated in angle-dependent spectra recorded with excellent statistics and a resolution of about 30 meV.[23]

The main features of the electron spectra are easily related to the characteristic properties of this system. These are the rather strongly attractive entrance channel potential that allows access to regions where bonding in the exit channel sets in, and an exponential-shaped width of a strength that leads to ionization probabilities (opacities) of about 80%. Thus, the spectrum stretches over more than 3 eV and comprises contributions from nuclear angular momenta ranging up to about 60. Its high-energy part shows the sharp rovibrational structure typical for associative ionization. The low-energy part due to Penning ionization exhibits the familiar Airy pattern with a supernumerary rainbow structure connected with a minimum in the difference potential. This is further modulated by a rapidly oscillating term caused by the in–out interference of heavy particle motion in the entrance channel. The gross structure of the Penning part can be well explained by a semiclassical treatment,[10,68] e.g., the damping of the rainbow structure has been shown to be due to the fact that the imaginary part of the entrance channel nuclear wave function is out of phase with respect to the real part by $\pi/2$. All these patterns are very pronounced in individual J con-

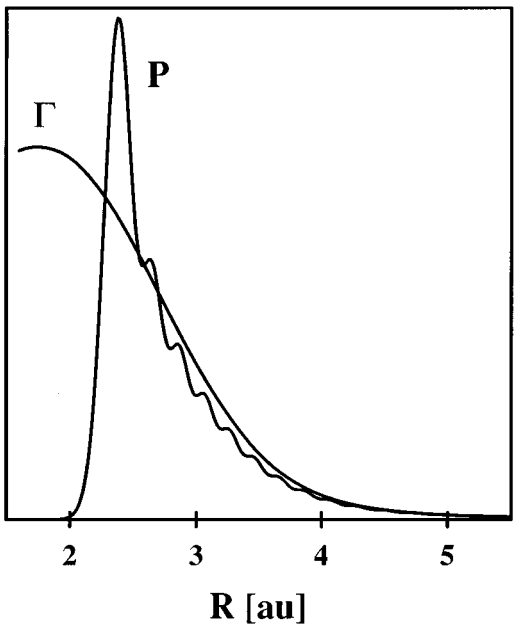

FIG. 11. Autoionization rate $P(R)$ and total width $\Gamma(R)$ as a function of internuclear separation, arbitary units.

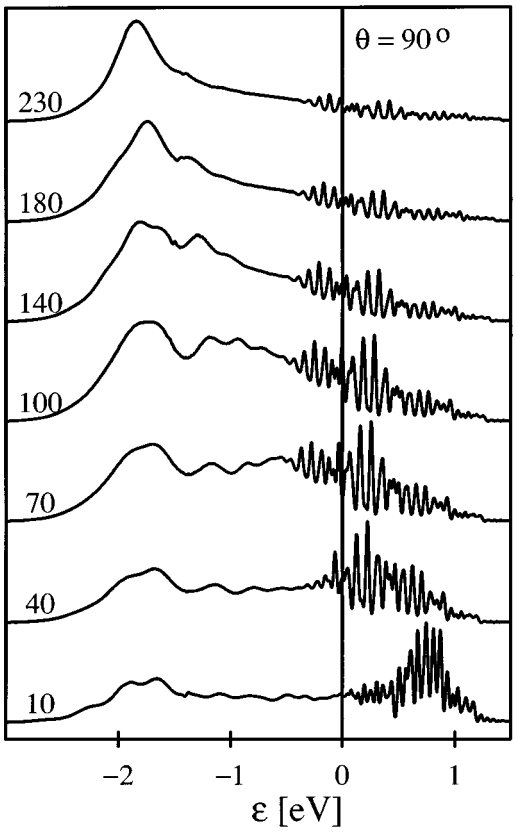

FIG. 12. Calculated electron spectra at 90° for selected collision energies.

tributions to the spectrum but, once the sum over J is made, they are progressively washed out with increasing collision energy E_{rel}. The variation of the spectral shapes with E_{rel} is, indeed, mainly due to the change of the range of contributing angular momenta J. This variation is, of course, difficult to investigate experimentally due to the inherently broad energy distribution in effusive atomic beams, but it can easily be accessed in calculations. In Fig. 12, we present calculated spectra for collision energies ranging from 10 to 230 meV for a single observation angle of 90°. With increasing collision energies, the associative parts of the spectra are gradually shifted to higher rovibrational levels and, at the same time, diminish as compared to the corresponding Penning parts. In between, there is sizable ionization into quasibound cation states.

Along with their measurements, Waibel *et al.*[15] presented the most detailed theoretical analysis so far. Their quantum scattering calculations were based on the approximate Eq. (43) for angle-integrated spectra, which implies the $\Delta J = 0$ restriction, using a preliminary version of our potential and model width functions. The results were directly related to the spectra taken under 90° perpendicular to the collision plane, owing to the widely held belief that such an attractive Penning system should emit electrons more or less isotropically.[15,65] Very good agreement could indeed be obtained for the associative part of the spectrum and a convincing picture of the J composition of the electron spectra evolved: Because of the exponential rise of the width function with decreasing separation, the turning point region is most efficient and associative ionization is mainly linked to low J values, while the main Airy peak of the PI part is built up mainly from high-J contributions. This analysis is fully corroborated by our present calculations. However, the interference structure of the PI part turned out incompatible with any of the realistic width functions tried in Ref. 21. The best-fit width, which was finally adopted, has a rather unrealistic shape and must be considered an inappropriate attempt to model effects of the neglected angular momentum transfer into the shape of the width function.

B. The angle dependence of the electron spectra

The analysis of the coupling elements in Sec. IV D has shown that there is sizable angular momentum transfer to the emitted electron. Significant terms V_l range up to $l=4$ and create, taken as function of internuclear distance, a characteristic pattern in the complex plane as seen in Fig. 2. The internal angular distributions (Fig. 5), therefore, turned out strongly anisotropic, being dominated by $l=2$ electrons for the most efficient internuclear distances around $2.4a_0$. As argued in Sec. II B, the ionizing collisions are sufficiently direct, even for attractive resonance states so that the anisotropy of the internal distribution should be visible in angular-dependent electron spectra. Spectral features that are particularly related to the electron emission (or observation) angle are best demonstrated on the basis of spectra for single collision energies. Theoretical angle-dependent electron spectra for the single collision energy $E_{\mathrm{rel}}=50$ meV are shown in Fig. 13. The spectra in forward and backward directions are more structured and modulated than the 90° spectrum with significant differences in the Penning part as well as in the

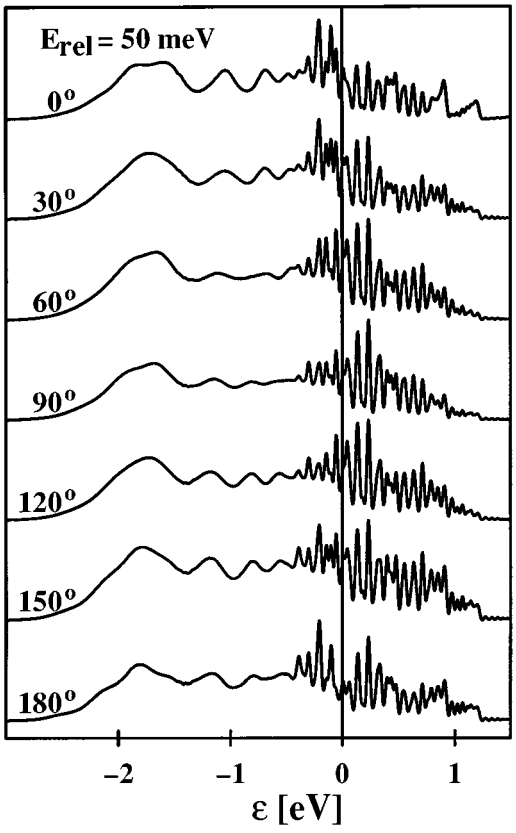

FIG. 13. Calculated electron energy spectra at different detection angles for $E_{\mathrm{rel}}=50$ meV. The electron energy is defined relative to the ''nominal'' energy at which an electron would be emitted in the separated atom limit.

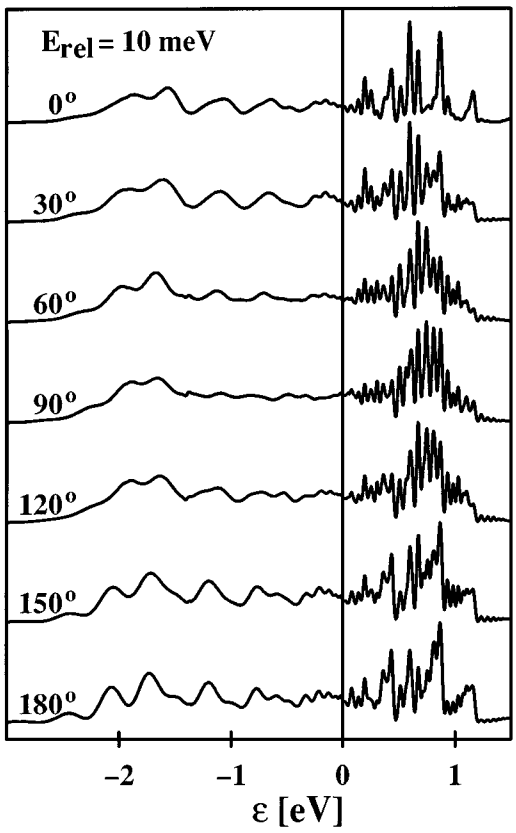

FIG. 14. Same as Fig. 13 for collision energy $E_{\mathrm{rel}}=10$ meV.

quasiassociative and associative part of the spectrum. The main Airy peak is shifted towards lower energies when going from 0° (forward) to 180° (backward) direction. This may be understood as a Doppler effect on the velocity of the electron emitted from the He moving in the forward direction, as concluded previously for repulsive systems such as rare-gas dimers.[35] Changes in the modulation in the main peak, as well as shifts of the secondary Airy peaks, are also clearly visible. The rich structure of the high-energy AI spectrum shows prominent steps in forward and backward directions that correspond to the onsets ($J^+=0$) of transitions to the vibrational levels $v=2$ and 3 of HeH^+. (The threshold for $v=1$ is not visible). These structures and their angle dependence are even more pronounced in the spectra for the lower collision energy $E_{\mathrm{rel}}=10$ meV, which are shown in Fig. 14. Note that, in this case, the relative weight of the PI is also lower. The backward spectra are now more structured than the forward ones, but again the 90° spectrum is the one with least modulation.

According to Eq. (34) for double differential cross sections, one can see that the amplitudes are given by coherent superpositions of all the J and l contributions. The individual terms contain phase factors from the electronic coupling matrix elements and from the radial wave function for the entrance channel, respectively, and depend via l (and M) on the electron emission angle θ. The delicate interplay between these various phase factors and the stationary phase conditions leads to the angular dependence of the observed electron spectra. Looking at the radial integrals involved, one should expect that rotational excitation or deexcitation during the autoionization process leads to shifts of the electron spectra towards lower and higher energies, respectively, because the points of stationary phase are, indeed, rather different for the integrals involving different J^+ and the same J. Due to this intricate way in which the electronic coupling enters the spectra, it is hard to rationalize the interference pattern from Eqs. (34) or (35). From the latter, it can be deduced that only even L contribute to the differential cross section at $\theta=90°$ and that the forward–backward asymmetry is solely due to odd L, i.e., a combination of even and odd components V_l. Thus, the dominance of the coupling terms V_0 and V_2 is reflected in the fact that the spectra in forward and backward direction, respectively, are rather similar in shape but differ clearly from the spectra for perpendicular detection. The latter should most closely resemble the angle-integrated spectrum since contributions from $L\neq 0$ cancel to a large extend at 90°. By means of classical trajectory calculations,[66] it has been demonstrated that the orientation of autoionizing quasimolecules with $J'=0-5$ at around the turning points is confined to a rather narrow angular range of about $\pm 25°$ around the relative velocity direction. From the observation that the internal angular distribution is strongly forward/backward peaked in the turning point region. [Fig.

6(a)], it can be understood that the high-energy end of the associative spectrum and, in particular, the onsets of vibrational channels are pronounced in forward and backward directions.

C. Collision energy distributions and comparison with experiment

Since the electron spectra were considered to be more or less isotropic, all Penning ionization electron spectroscopy studies of the He*+H collisional complex, except the most recent one,[23] have been performed using an experimental setup involving crossed atomic beams and a spectrometer at right angles to the beam directions. Merz *et al.*[23] used for the first time a rotatable spectrometer to detect electrons and ions in the plane determined by the atomic beams. They used a mildly supersonic discharge source to obtain the well-collimated metastable He*(^3S) beam (divergence $<1°$). Based on experiments with an earlier but similar source, the velocity distribution has been specified in Ref. 17 as that of a nozzle beam, i.e., $\propto v^2 \exp[-(m/2kT)\cdot(v-u)^2]$ with the central velocity $u=1639$ m/s and an effective temperature of $T=19.4$ K. A quite recent analysis for heavier rare-gas atoms has revealed that the distribution is likely to be somewhat broader and shifted to higher energies. As suggested by the experimentalists,[70] all following calculations are, therefore, done using $u=1750$ m/s and $T=26$ K. (Note, however, that these changes do not influence the final result very much since the relative energy distribution is mainly determined by the properties of the H beam.) For the atomic hydrogen beam, on the other hand, they used an effusive, rather divergent source ($\pm 15°$) with a Maxwellian velocity distribution corresponding to an estimated temperature of $T=300$ K.

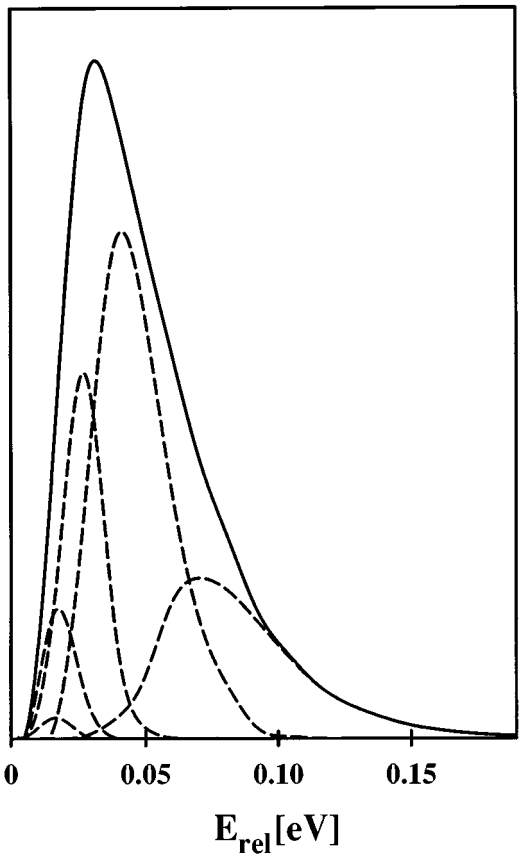

FIG. 15. Collision energy distribution $f_\alpha(E_{\mathrm{rel}})$ for the experiment of Ref. 23. Broken lines: effective energy distributions for collisions that are sampled under the relative velocity directions that deviate from the mean relative velocity direction by 15°, 0°, −15°, −30°, and −45°, respectively (from right to left). These are used for the simulation of the in-plane measurements. Solid line: total energy distribution, used for 90° detection angle perpendicular to the plane of the atom beams.

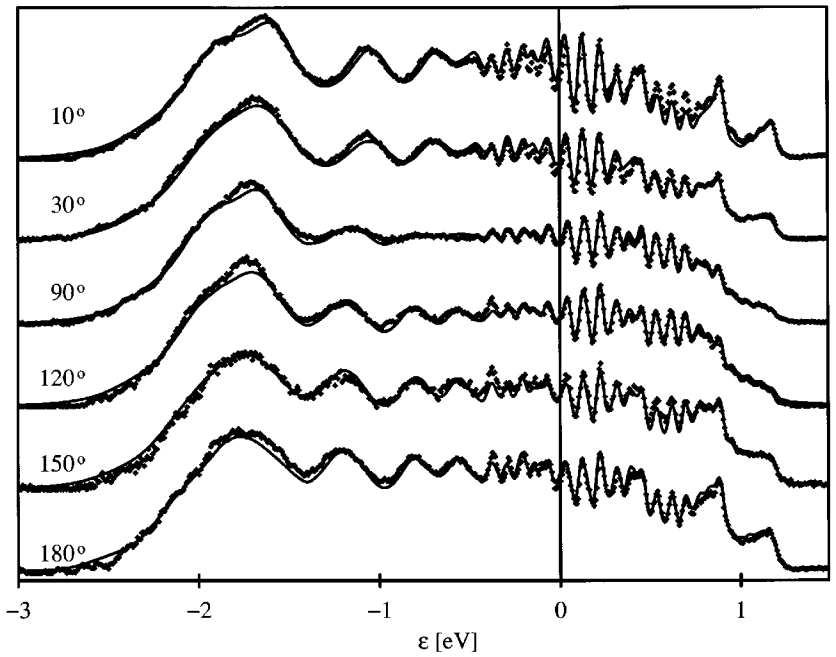

FIG. 16. Measured (+) and calculated (solid line) electron spectra for different detection angles.

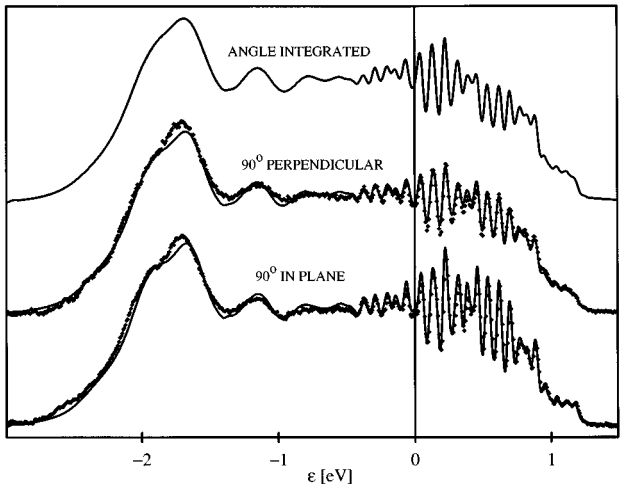

FIG. 17. Measured (+) and calculated (solid line) electron spectra for detection at 90° perpendicular to the plane of the beams and 90° in-plane, as compared to the calculated angle-integrated spectrum.

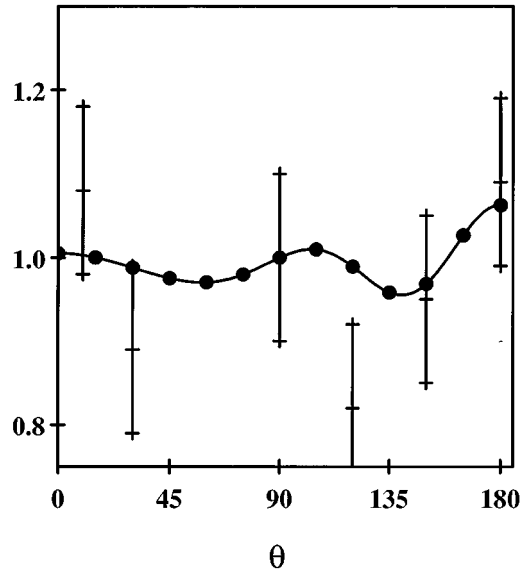

FIG. 18. (Energy integrated) angular differential ionization cross section relative to 90°. Solid line: calculated; and bars: experimental integrated intensities with estimated uncertainties, see Ref. 71.

Disregarding the deviations due to the beam divergences, electrons collected perpendicularly to the plane of the beams are all ejected perpendicularly to the relative velocity vector of the colliding atoms. The situation is quite different for in-plane measurements, for which the detection angle is usually defined with respect to the mean relative velocity vector. Since the latter may be at an angle α to the actual relative velocity vector of a colliding pair, the actual emission angle of the detected electron is $\theta^a = \theta - \alpha$. For comparison with experiment, the spectra calculated for emission angles θ^a have, therefore, to be folded by the distribution of α. This can be combined with the folding for the energy distribution by deriving effective energy distributions $f_\alpha(E_{\mathrm{rel}})$ for relative velocities with a common directional deviation α. Figure 15 shows such energy distributions for directional deviations that are multiples of 15°. The sum of these distributions, also shown, is appropriate for the detection angle perpendicular to the plane of the atom beams.

In Fig. 16, we compare our theoretical spectra, properly averaged over collision energies, with the experimental spectra obtained by Merz[71] and Merz and co-workers.[23,25] For a given detection angle, both spectra are here normalized to the same integral value (see Fig. 18 for their relative norms). The overall agreement is very satisfactory. The theoretical spectra indeed reproduce all features observed in the experiments. We stress, in particular, that the agreement in the low-energy wing of the main Airy peak proves that the minimum of the resonance potential is correct to within experimental resolution. The relative strength of the AI parts verify that the turning points of the entrance channel motion are accurately located with respect to the cation potential. The agreement in the angular dependence, even of faint details, of the interference structures demonstrates that the strength and phases of the coupling elements are sound.

In Fig. 17, the theoretical angle-integrated spectrum is compared with the calculated and measured spectra for 90° perpendicular and 90° in-plane detection. The sharp modulation of the AI part of the 90° perpendicular spectrum is more pronounced than for the 90° in-plane spectrum, which is subject to additional averaging. The angle-integrated spectrum is seen to resemble most closely the 90° perpendicular spectrum, giving some justification to the usual identification of the latter with model spectra from integral–spectra formulas. This is related to the fact that odd-L terms do not contribute to either of them and that integration over θ gives maximal weight to the 90° regime.

Finally, the energy-integrated angle-dependent cross section is presented in Fig. 18. Experimental values together with the error bars as obtained by Merz[71] are also shown. Obviously, little angular dependence survives the energy integration, that is, the largest deviation from average is +6%

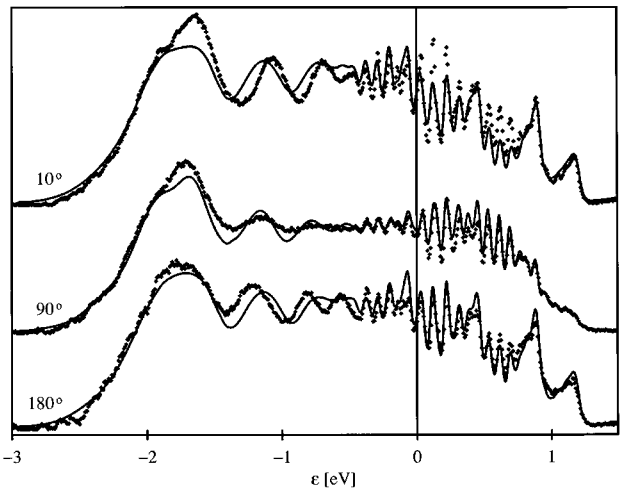

FIG. 19. Calculated electron spectra compared to measured (+) ones with odd terms $l = 1,3$ being dropped.

at 180°. Our angle dependence is much weaker than that suggested in Ref. 23 on the basis of a symmetrical fit around 90°.

As to the significance of the size and phase of the l components of the coupling, we would like to point out that the interference pattern changes drastically when modifications are made. An example is given in Fig. 19 for which the seemingly small odd components for $l=1,3$ have been dropped. Not only the opposite shifts of the Airy oscillations in forward and backward direction are missed, but the spectrum at 90° also suffers from the missing odd $l_1=l_2$ contributions.

VI. CONCLUSIONS

We have presented a detailed account of *ab initio* computational procedures that appear to provide an adequate treatment for a large class of autoionizing molecular collision complexes. These are characterized by core-exited resonance states as they, e.g., evolve from metastable states of excited rare-gas atoms. Feshbach projection is then easy to implement in CI codes and yields accurate resonance potentials, as well as a convenient access to the resonance-to-continuum coupling via the ''Penning MO,'' representing the source of continuum electrons. This L^2 MO can, in a second step, be expanded in terms of the solutions of the electron scattering problem in the exit channel, which, in our case, were obtained by coupled channel calculations in static-exchange approximation. The absence of threshold electrons allows considering autoionization as a vertical process characterized by the resonance condition on electron energy. This leads to a local complex potential for the resonance state dynamics and local complex coupling elements to continuum states, which correlate asymptotically to electrons of particular angular momentum. These coupling elements are directly linked to the internal angular distribution of the electrons, and the interplay of their phases with those acquired in the heavy particle motion determines the dependence of electron spectra on the detection angle. The theoretical electron spectra, after convolution with the proper collision energy distribution, are in very satisfying agreement with high-resolution electron spectra measured recently, not only for the fundamental system considered in detail here, $He^*(2s^3S)+H(1s)$, but also for the case of $He^*(2s^1S)+H(1s)$ (which is rather different in terms of resonance potential and coupling elements) and the related systems where H is substituted by D.[25,26] Further investigations of collision complexes for He* with alkali atoms are under way and their preliminary results support the conclusion that a purely *ab initio* treatment as exemplified here is capable of producing reliable electron spectra even for cases where they exhibit a rich interference structure. The nice agreement in all details demonstrated above may, thus, be taken as experimental evidence that the calculated coupling elements are sound.

ACKNOWLEDGMENTS

This work has been supported in part by the Deutsche Forschungsgemeinschaft. The authors are indebted to H. Hotop for numerous stimulating discussions.

[1] F. M. Penning, Naturwissenschaften **15**, 818 (1927).
[2] P. E. Siska, Rev. Mod. Phys. **65**, 337 (1993).
[3] C. K. Rhodes, IEEE J. Quantum Electron. **10**, 153 (1974).
[4] M. B. McElroy, Planet. Space Sci. **13**, 403 (1965).
[5] J. Weiner, F. Masnou-Seeuws, and A. Giusti-Suzor, Adv. At. Mol. Phys. **26**, 209 (1990).
[6] H. Feshbach, Ann. Phys. (N.Y.) **5**, 357 (1958); **19**, 287 (1962).
[7] T. F. O'Malley, Phys. Rev. **150**, 14 (1966).
[8] H. Nakamura, J. Phys. Soc. Jpn. **26**, 1473 (1969).
[9] W. H. Miller, J. Chem. Phys. **52**, 3563 (1970).
[10] R. J. Bieniek, Phys. Rev. **18**, 392 (1978).
[11] W. Domcke, Phys. Rep. **208**, 97 (1991).
[12] H. Morgner, Chem. Phys. **145**, 239 (1990).
[13] W. H. Miller, C. A. Slocomb, and H. F. Schaefer III, J. Chem. Phys. **56**, 1347 (1970).
[14] A. P. Hickman, A. D. Isaacson, and W. H. Miller, J. Chem. Phys. **66**, 1483 (1977).
[15] H. Waibel, M.-W. Ruf, and H. Hotop, Z. Phys. D **9**, 191 (1988).
[16] M.-W. Ruf, A. J. Yencha, and H. Hotop, Z. Phys. D **5**, 9 (1987).
[17] M. W. Müller, A. Merz, M.-W. Ruf, H. Hotop, W. Meyer, and M. Movre, Z. Phys. D **21**, 89 (1991).
[18] W. Meyer, J. Chem. Phys. **64**, 2901 (1976); H.-J. Werner and E.-A. Reinsch, *ibid.* **76**, 3144 (1982).
[19] P. W. Langhoff, Int. J. Quantum Chem. Symp. **8**, 347 (1974).
[20] A. U. Hazi, J. Phys. B **11**, L259 (1978).
[21] A. Merz, M. W. Müller, M.-W. Ruf, H. Hotop, W. Meyer, and M. Movre, Chem. Phys. **145**, 219 (1990).
[22] A. Merz, M. W. Müller, M.-W. Ruf, H. Hotop, W. Meyer, and M. Movre, Chem. Phys. Lett. **165**, 377 (1989).
[23] A. Merz, M.-W. Ruf, and H. Hotop, Phys. Rev. Lett. **69**, 3467 (1992).
[24] Vo Ky Lan, M. Le Dourneuf, and J. M. Launay, in *Electron–Atom and Electron–Molecule Collisions*, edited by Juergen Hinze (Plenum, New York, 1983).
[25] A. Merz, M.-W. Ruf, H. Hotop, M. Movre, and W. Meyer, J. Phys. B **27**, 4973 (1994).
[26] M. Movre, W. Meyer, A. Merz, M.-W. Ruf, and H. Hotop, Chem. Phys. Lett. **230**, 276 (1994).
[27] W. H. Miller and H. F. Schaefer III, J. Chem. Phys. **53**, 1421 (1970).
[28] A. D. Isaacson and W. H. Miller, Chem. Phys. Lett. **62**, 374 (1979).
[29] M. Movre and W. Meyer, Proceedings of the International Conference on the Physics of Electronic and Atomic Collisions, Abstracts (1993).
[30] B. K. Sarpal, J. Phys. B **26**, 4145 (1993).
[31] H. Morgner, J. Phys. B **11**, 269 (1978).
[32] V. Hoffmann and H. Morgner, J. Phys. B **12**, 2857 (1979).
[33] A. P. Hickman and H. Morgner, J. Phys. B **9**, 1765 (1976).
[34] R. J. Bieniek, J. Phys. B **7**, L266 (1974).
[35] A. Niehaus, Adv. Chem. Phys. **45**, 399 (1981).
[36] A. U. Hazi and H. S. Taylor, Phys. Rev. A **1**, 1109 (1970).
[37] L. Lipsky and A. Russek, Phys. Rev. **142**, 59 (1966).
[38] E. O. Steinborn and F. Eckhard, Theor. Chim. Acta **52**, 189 (1979).
[39] A. K. Bhatia and A. Temkin, Phys. Rev A **13**, 2322 (1976).
[40] A. K. Bhatia, Phys. Rev. A **18**, 2523 (1978).
[41] R. Junker, Phys. Rev. A **18**, 2437 (1978).
[42] A. Temkin, A. K. Bhatia, and J. N. Bardsley, Phys. Rev. A **5**, 1663 (1972).
[43] D. G. Hummer and D. W. Norcross, Bull. Am. Phys. Soc. **24**, 1183 (1979).
[44] A. L. Sinfailam and R. K. Nesbet, Phys. Rev. A **6**, 2118 (1972).
[45] B. F. Davis and K. T. Chung, Phys. Rev. A **29**, 1878 (1984).
[46] H. Ehrhardt, L. Langhans, and F. Linder, Z. Phys. **214**, 179 (1968).
[47] S. Cvejanovic, J. Comer, and F. H. Reed, J. Phys. B **7**, 468 (1974).
[48] D. E. Golden, F. D. Schowengerdt, and J. Macek, J. Phys. B **7**, 468 (1974).
[49] R. E. Kennerly, R. J. Van Brunt, and A. C. Gallagher, Phys. Rev. A **23**, 2430 (1981).
[50] P. Ziem, R. Bruch, and N. Stolterfoht, J. Phys. B **8**, L480 (1975).
[51] D. Rassi, V. Pejcev, and K. J. Ross, J. Phys. B **10**, 3535 (1977).

[52] M. Rodbro, R. Bruch, and P. Bisgaard, J. Phys. B **12**, 2413 (1979).
[53] B. R. Johnson, J. Chem. Phys. **67**, 4086 (1977), and references therein.
[54] S. Huzinaga, J. Chem. Phys. **42**, 1293 (1965).
[55] C. L. Pekeris, Phys. Rev. **126**, 1470 (1962).
[56] G. A. Victor, A. Dalgarno, and A. J. Taylor, J. Phys. B **1**, 13 (1968).
[57] C. L. Pekeris, B. Schiff, and H. Lifson, Phys. Rev. **126**, 1057 (1962).
[58] A. Dalgarno and G. A. Victor, J. Chem. Phys. **49**, 1982 (1968).
[59] T. R. Proctor and W. C. Stwalley, J. Chem. Phys. **68**, 5292 (1978).
[60] D. Spelsberg and W. Meyer, J. Chem. Phys. **99**, 8351 (1993).
[61] H. Morgner and A. Niehaus, J. Phys. B **12**, 1805 (1979).
[62] I. Paidarova, J. Vojtik, and R. Polak, J. Chem. Phys. **72**, 119 (1982).
[63] D. M. Bishop and L. M. Cheung, J. Mol. Spectrosc. **75**, 462 (1979).
[64] W. Kolos and J. M. Peek, J. Chem. Phys. **12**, 381 (1976).
[65] T. Ebding and A. Niehaus, Z. Phys. **270**, 43 (1974).
[66] A. Merz, M.-W. Ruf, H. Hotop, M. Movre, and W. Meyer, The Physics of Electronic and Atomic Collisions, XVIII International Conference, Aarhus, Denmark (1993), edited by T. Andersen, B. Fastrup, F. Folkmann, H. Knudsen and N. Andersen [AIP Conf. Proc. **295**, 852].
[67] *Atomic Data for Fusion, Vol. 1*, edited by C. F. Barnett (Oak Ridge National Laboratory, 1990).
[68] J. Bieniek, M. W. Müller, and M. Movre, J. Phys. B **23**, 4521 (1990).
[69] R. H. Neynaber and S. Y. Tang, J. Chem. Phys. **69**, 4851 (1978).
[70] H. Hotop (private communication).
[71] A. Merz, dissertation, Universität Kaiserslautern (Verlag Shaker, Aachen 1993).